Redox–state Dependent Activation of Silanes and Ammonia with Reverse Polarity ($PC_{carbene}P$)Ni Complexes: Electrophilic vs. Nucleophilic Carbenes†

Etienne A. LaPierre, Warren E. Piers*, and Chris Gendy.

A rigidified $PC_{alkyl}P$ ligand allowed for the synthesis and charactarization of cationic and radical $PC_{Carbene}P$ nickel complexes in which the carbene anchor of the pincer framework is electrophilic rather than nucleophilic. Alpha-hydride abstraction from ($PC_{alkyl}P$)nickel halide complex readily leads to the cationic carbene complex, which furnishes the radical carbene complex by one electron reduction. The reactivity of these reverse polarity carbene complexes towards small molecules (H_2, CO, CO_2, R_3SiH, NH_3) reveals different modes of activation when compared to previously reported nucleophilic nickel carbene complexes, and a clear dependence on the redox state of the complex. For H_2, CO and CO_2, no reaction is observed, but silanes react via hydride transfer and formation of solvated silylium ions. Ammonia is activated in a novel way, wherein it coordinates the carbene carbon and is deprotonated to form a robust C-N bond. This is not only a rare example of ammonia activation by a first row transition metal but also evidence of the intermediacy of group 10 carbenes in direct C-N bond forming reactions.

Introduction

The activation of small molecules is a key step in many organometallic mediated chemical transformations. In addition to fundamental metal-centred processes like oxidative addition[1, 2] or sigma bond metathesis,[3] activation of bonds through metal-ligand cooperation has emerged as an additional tool for challenging bond cleavages.[4] Numerous design principles exist for ligands capable of participating in cooperative substrate activation,[4-9] including pincer-supported pyridine rings prone to undergo dearomatization-aromatization, ligands containing a basic amide functionality able to accept electrophiles, and the incorporation of a reactive carbene moiety in the ligand scaffold,[10, 11] which may behave as nucleophiles (Schrock type) or electrophiles (Fischer type) depending on the polarity of the M=C bond.

Examples of nucleophilic type M=C ligand cooperating carbenes include our previously reported $PC_{carbene}P$ Ni complexes **I**[12] and **II**[13] (Chart 1); these species are competent in the activation of a wide variety of substrates *via* metal-ligand cooperation between the nickel center and the nucleophilic and basic carbene carbon,[12, 14, 15] as are closely related palladium complexes.[16-19] Inspired by reports of the accessibility of formally oxidized palladium carbenes **III** and **IV**, systems containing electrophilic and radical carbene fragments, respectively, through redox chemistry in analogous $PC_{carbene}P$ palladium complexes,[20] we sought to access related nickel complexes through more direct synthetic routes. Considering the importance of Pt[21] and Pd[22] carbenes as intermediates in catalytic organic transformations, along with current emphasis on the use of earth abundant metal complexes and the potential for one electron catalytic steps, and given the clear effect of both metal and carbene polarity in reactivity,[23, 24] we sought to explore the electronic structure of the electrophilic and radical Ni carbene complexes and examine their competency in small molecule activation. For this purpose, we chose to employ the more rigid PCP pincer framework **II** due to its superior stability compared to unlinked systems,[13] as well as the clear demonstrated capability of rigid pincer platforms to support highly reactive Ni complexes.[25]

Chart 1. Select Group 10 Carbene Complexes

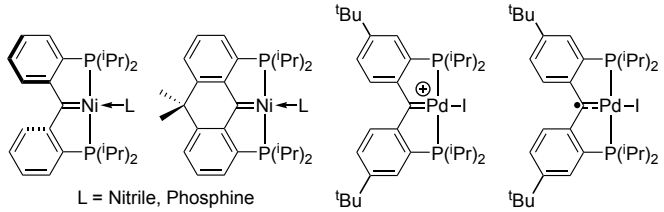

Despite recent advances,[11, 26] Group 10 cationic carbene complexes are generally transient species, with a limited number of isolable examples.[20, 27-30] As a result, reactivity studies have been largely limited to ylide formation and reactions with alkali metal salts;[20, 27] reactivity with small

molecules, apart from hydrogen, remains largely unexplored. Herein, we report the synthesis and redox behaviour of nickel analogs of compounds **III** and compare the reactivity of these reverse polarity carbenes with their nucleophilic analogues **II** towards small molecules.

Results and Discussion

Treatment of previously reported ($PC_{alkyl}P$)NiBr complex **1**[13] with $[CPh_3]^+[SbF_6]^-$ cleanly leads to cationic carbene complex **2** *via* α-hydride abstraction[30] (Scheme 1). The $^{13}C\{^1H\}$ NMR spectra complex **2** features a characteristic triplet at 250.8 ppm ($^3J_{P\text{-}C}$ = 9.6 Hz) consistent with a Fisher-type carbene complex and far downfield of the signal observed at 114.5 for the carbene carbon in the Schrock type analogue **II** (L = NC^tBu).[13] Its formulation as a cationic carbene compound was confirmed via determination of its molecular structure (Fig. 1).

Scheme 1. Synthesis of Complex **2**

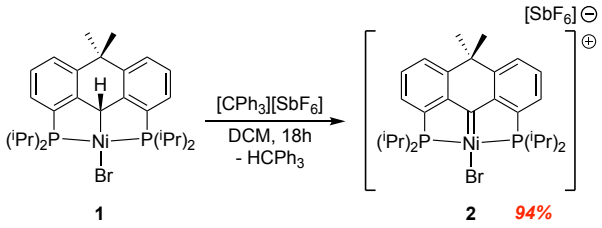

The solid-state structure of **2** (Fig. 1, top) reveals a short Ni-$C_{carbene}$ bond of 1.874(1) Å, notably shorter than the Ni-C distance of 1.974(2) Å in **1**,[13] or that of 1.906(1) Å in nucleophilic analog **II**,[13] though longer than that of Hillhouse's three coordinate Ni carbene complex.[31] This bond contraction in **2** vs **II** is consistent with a depopulation of a Ni-C orbital that is π* antibonding in character (*vide infra*). Also notable is the small torsion angle (8.77°) between the planes defined by the aryl rings of the ligand backbone compared to **1** and **II**, which may be evidence of π-stabilization of the carbene moiety by the aryl rings. DFT calculations (B3PW91/SDD(Ni)/6-31G**, Fig. 1, bottom) of the cationic fragment reveals a largely ligand centered π*-type LUMO, in contrast, in **II** this π* type orbital is the fully populated HOMO (Fig. S1). As such, **2** can be viewed as the $2e^-$ oxidation product of **II**, and may be expected to display largely ligand centered, electrophilic reactivity, in contrast to the ligand nucleophilicity of **II**.

Scheme 2. Reduction Chemistry of **2**

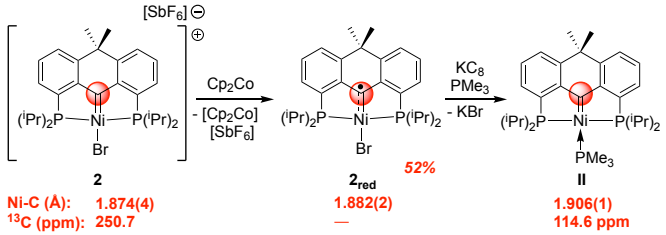

The cyclic voltammogram of **2** in THF revealed two independent reduction events (Fig. 2), one reversible wave at -0.43 V (vs. Fc/Fc^+) and an irreversible reduction event at -2.0 V,

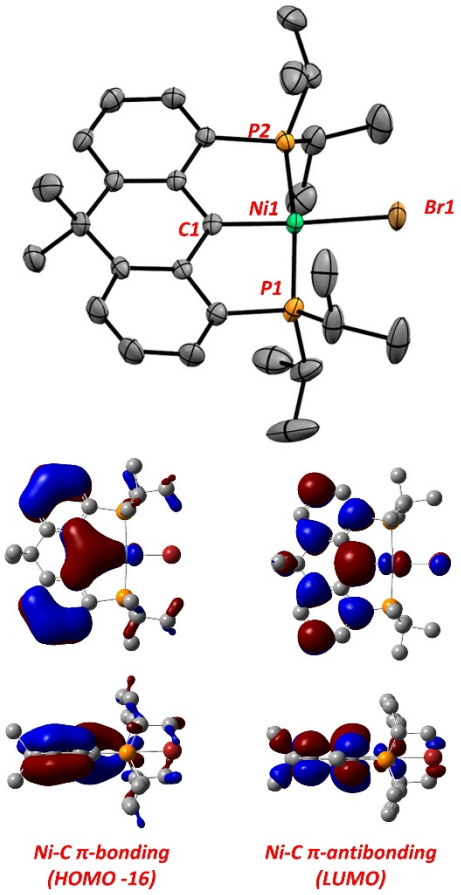

Figure 1. ORTEP diagram for complex 2(top), DFT Calculated Molecular Orbitals of 2 (bottom). Thermal ellipsoids are shown at the 50% probability level. Hydrogen atoms and counter anion are omitted for clarity. Select bond lengths (Å) and angles (degrees) for 2: Ni1-C1 1.874(4), Ni1-Br1 2.333(2), P2-Ni1 2.194(2), P1-Ni1 2.203(2), C1-Ni1-Br1 174.9(1), P2-Ni1-P1 171.49(6). For full computational details see ESI.

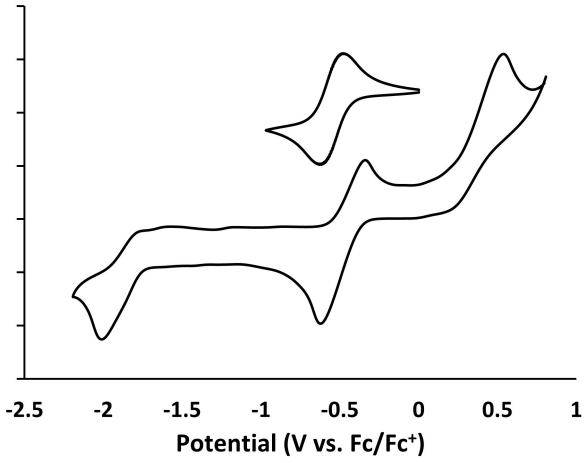

Figure 2. Cyclic Voltammogram for 2. Inset: Highlight of First Reduction Potential. 0.1M [NBu4][PF6], 1mM **2**, THF, 100 mV/s, Pt working electrode.

similar to previously reported palladium complex **III** (-0.38 and 2.03 V vs. Fc/Fc^+), which is indicative of only slight metal effects. Accordingly, treating **2** with one equivalent of cobaltocene resulted in the immediate conversion to radical carbene complex $\mathbf{2_{red}}$, while further reduction with 1 equivalent of the stronger reductant KC_8 in the presence of PMe_3 led to **II** (Scheme 2). Compound $\mathbf{2_{red}}$ is paramagnetic, with no distinct features in either the ^1H or ^{31}P NMR spectra. A magnetic moment measurement using the Evans method revealed a ground state magnetic moment of 1.72 μ_B consistent with an S = ½ spin state. Solutions of complex $\mathbf{2_{red}}$ are highly sensitive to oxygen, though it is stable for months in the solid state under inert conditions. The EPR spectrum (toluene glass, 128K, Fig. S2) exhibits a $g \approx 2.04$, consistent with and organic centred radical and not a Ni(I) species. Direct synthesis of $\mathbf{2_{red}}$ by H-atom abstraction from complex **1** by 2,4,6-tritertbutylphenoxy radical did not lead to significant consumption of **1** by ^1H NMR spectrometry, leaving reduction of **2** as the only viable synthetic pathway to $\mathbf{2_{red}}$.

Like **2**, the solid-state structure of $\mathbf{2_{red}}$ shows a planar arrangement of the aryl rings (C_{aryl} torsion = 2.51˚) (Fig. 3), indicative of potential delocalization throughout the π-system; further, the Ni-C bond length of 1.882(2) is intermediate between that of **II** and **2**, consistent of partial occupation of a π* type orbital. The DFT calculated α-SOMO of $\mathbf{2_{red}}$ (Fig. 3) is strikingly similar to the LUMO of **2** (Fig. 2), indicating a largely ligand centered, highly delocalized radical, consistent with the EPR spectrum. Unlike some previously reported palladium radical carbenes,[32] no dimerization through the position on the ligand *para* to the carbene carbon was observed, despite the steric availability of the site and the presence of singly occupied orbital density on this carbon. $\mathbf{2_{red}}$ is remarkably stable, exhibiting no reaction with 1 atmosphere of either CO_2 or NH_3 at 80°C for multiple days, and only trace conversion (<5% relative to silane) to **1** when treated with 10 eq. of $HSiMe_2Ph$ at 80°C for three days. ‡

Noting an irreversible oxidation couple at 0.53V (vs. Fc/Fc^+) in the CV of **2** (Fig. 2), chemical oxidation of **2** was also explored. Attempts to oxidize **2** using the strong oxidizing agent Magic Blue ($E_{1/2}$ = 0.70 in DCM)[33] showed no spectroscopic evidence of reaction. Furthermore, no formation of *tris*-(4-bromophenyl)amine was observed, which suggests no reduction of the oxidant took place, and the lack of spectroscopic change in **2** was not simply due to product instability and decomposition to return the starting materials. However, treatment of **2** with chemically non-innocent oxidants $ONMePh_2$ and PhINTs resulted in immediate consumption of **2** and formation of new C_s symmetric products, as indicated by both $^{31}P\{^1H\}$ and ^1H NMR spectrometry, along with concomitant formation of the corresponding amine and iodobenzene, respectively (Scheme 3).

Single crystal X-ray diffraction revealed that in the case of both oxidants the resulting product is that of group transfer from the oxidant to the carbene carbon, leading to ketonic product $\mathbf{3_O}$ and iminic product $\mathbf{3_{NTs}}$. This reactivity is reminiscent of previously reported reactions of diazo compounds with Pt(II) carbenes.[27] Product $\mathbf{3_O}$ contains a short C=O contact of 1.280(5) Å, closer to typical diaryl ketone (~1.23Å) than a C-O single bond,[34] and shorter than reported Ir and Ni

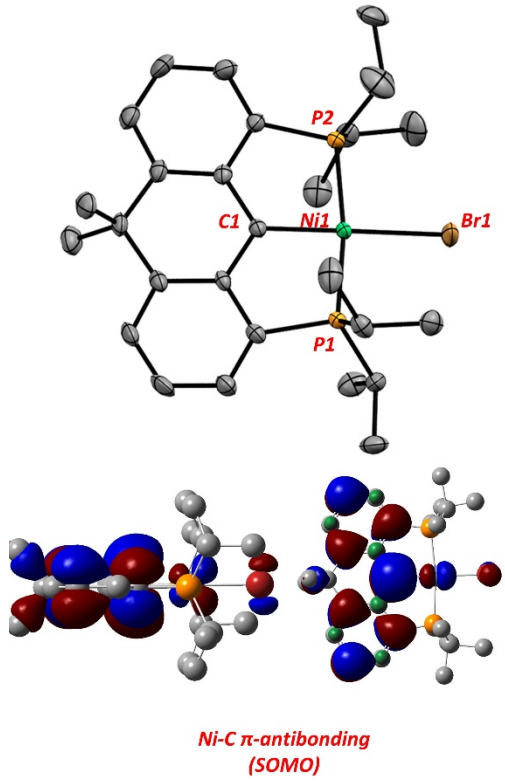

Figure 3. ORTEP diagram for complex 2_{red} (top), DFT Calculated Molecular Orbitals of 2_{red} (bottom). Thermal ellipsoids are shown at the 50% probability level. Hydrogen atoms are omitted for clarity. Select bond lengths (Å) and angles (degrees) for 3: Ni1-C1 1.882(2), Ni1-Br1 2.3390(3), P1-Ni1 2.1609(2), P2-Ni1 2.1568(8), C1-Ni1-Br1 177.08(7), P2-Ni1-P1 171.70(3). Dihedral angle C_{aryl}: 2.51°. For full computational details see ESI

metalloepoxides,[35-37] though roughly equal to a related Pd(0) complex.[38] In addition, the $^{13}C\{^1H\}$ NMR chemical shift of the C1 carbon is 182.8 ppm, typical of ketones, and downfield of aforementioned metallaepoxides. The lack of $^2J_{C\text{-}P}$ coupling,

Scheme 3. Oxidation Chemistry of **2**

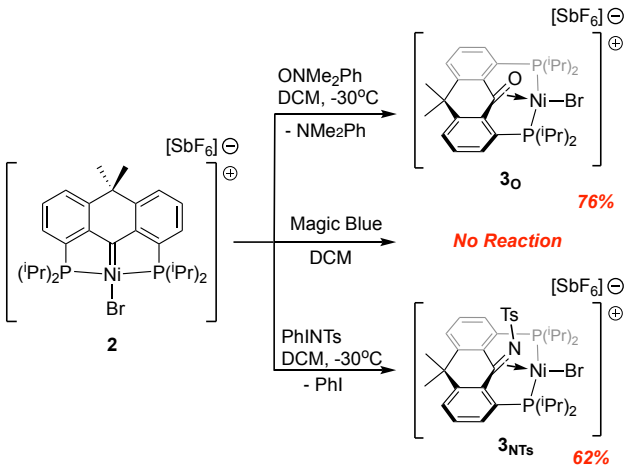

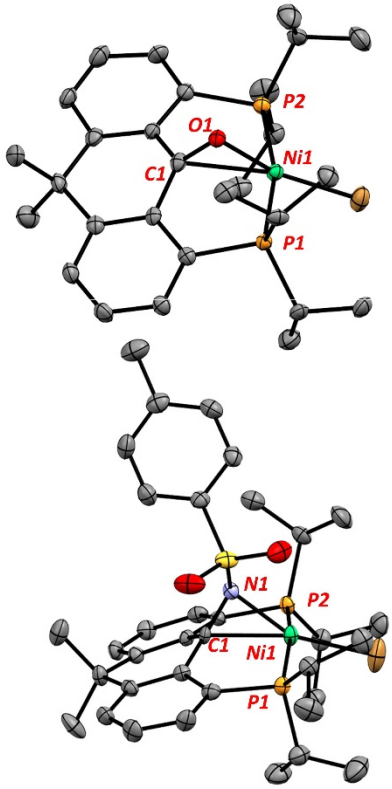

Figure 4. ORTEP diagrams for complexes 3_O (top) and 3_{NTs} (bottom). Thermal ellipsoids are shown at the 50% probability level. Hydrogen atoms and counter anions are omitted for clarity. Select bond lengths (Å) and angles (degrees) for 3_O: Ni1-C1 2.301(4), Ni1-O1 1.870(3), C1-O1 1.280(5), Ni1-Br1 2.2569(7), Ni1-C1-O1 54.3(2), Br1-Ni1-C1 161.4(1), Br1-Ni1-O1 164.74(9), P2-Ni1-P1 165.27(5), Br1-Ni1-"centroid: C1 O1" 176.24. Select bond lengths (Å) and angles (degrees) for 3_{NTs}: C1-Ni1 2.183(3), Ni1-N1 1.927(3), C1-N1 1.354(4), P1-Ni1-P2 163.40(4), Ni1-C1-N1 60.8(2), "centroid: C1 N1"-Ni1-Br1 175.73.

typically observed in $PC_{carbene}P$ and $PC_{alkyl}P$ complexes in these Ni PCP systems, is further indication of a weak Ni-C1 interaction, as is the long bond length of 2.301(4) Å. Therefore, we view $\mathbf{3_O}$ as an η^2-ketone. The complex $\mathbf{3_{NTs}}$ may also be viewed this way, although the elongated C-N bond distance of 1.354(4) Å is more typical of pyridines than of imines[34] and the $^{13}C\{^1H\}$ chemical shift of the iminic carbene is shifted upfield to 139.9 ppm from typical values of ~175 ppm for aryl tosylimines.[39] The Ni-C1 distance of 2.183(3) Å here is shorter than in $\mathbf{3_O}$ and at room temperature the ^1H NMR spectrum of $\mathbf{3_{NTs}}$ is indicative of C_s symmetry, as opposed to the C_1 symmetry the solid-state structure would indicate, suggesting rapid inversion at N1 at room temperature. Thus, the increased backbonding between Ni and the more electron withdrawing C=NTs group gives it more nickellaaziridine character. Nonetheless, both compounds can be viewed as being Ni(II) cations in which the ketone and imine moieties function as neutral η^2 donors. The clean oxidative group transfer chemistry to the carbene carbon observed here contrasts with observed oxidation of the phosphine arms in reactions of amine *N*-oxides with related $(PC_{alkyl}P)$Ni cations.[40]

Having examined the redox chemistry of cationic carbene **2**, we sought to its reactivity with small molecules with a view to making comparisons with the previously studied reactions with the nucleophilic carbenes exemplified by **I** and **II**[12, 14] and Hillhouse's coordinatively unsaturated terminal nucleophilic nickel carbene.[31, 36, 41] Additional substrates were chosen based on their demonstrated reactivity with isoelectronic Ir(I)[24, 35, 42-48] and cationic Pt(II) carbene complexes,[27] to explore potential metal effects.

Scheme 4. Reactions of **2** with Small Molecules

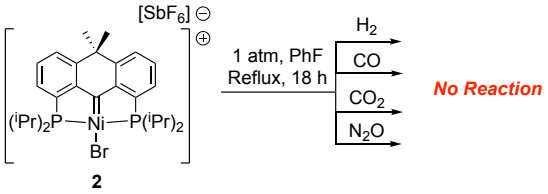

At room temperature complex **2** displays no reactivity with numerous substrates that have demonstrated reactivity with other carbene complexes, such as H_2, CO, CO_2 and N_2O (Scheme 4). As the ionic nature of **2** limits its solubility, fluorobenzene was used as an inert, non-coordinating solvent to effect more forcing temperatures and induce reactivity; however, none was observed even after prolonged heating. The lack of reactivity exhibited towards the latter three substrates, which readily react with nucleophilic Ni carbenes,[13, 31, 36] can be explained in part by their poor Lewis basicity, which prevents binding to the electrophilic carbene; further, the poor nucleophilicity of the metal precludes metal centered binding. The inability of **2** to add hydrogen across the Ni=C bond in a 1,2 fashion is curious, as isoelectronic, electrophilic, Ir(I)[42, 46-48] and Pt(II) carbenes[27] do so readily. This may be due to the relative inaccessibility of a higher oxidation state at nickel to facilitate hydrogen cleavage by oxidative addition. Ni(IV) species are rare and generally require some combination of hard, tridentate, facially coordinating, nitrogen ligands, chelating dianionic carbon ligands, and/or CF_3 ligands, and their formation is generally brought about by chemical oxidants.[49-54] To our knowledge there are no known examples of Ni(II)/Ni(IV) oxidative addition with hydrogen.

Further investigation of the ability of **2** to effect 1,2-addition of substrates across the carbene moiety was explored *via* reactivity of silanes. The proclivity of silanes to undergo 1,2 addition with group 10 carbenes such as **I** and analogous Pd complexes is well documented,[14, 19] with studies revealing not only the possibility concerted 1,2-addition of the Si-H bond across the metal carbene bond to yield metal hydride species,[14, 19] but also reverse polarity addition leading to 5-coordinate silyl compounds, depending on the coordination environment of the metal.[19] In contrast, treatment of **2** with excess $HSiMe_2Ph$ in THF leads to neither the formation of a nickel hydride or silyl complex, but the near quantitative reformation of **1** by $^{31}P\{^1H\}$ NMR and release of $FSiMe_2Ph$, as noted by a sharp singlet at -163.0 ppm in the $^{19}F\{^1H\}$ NMR spectrum;[55] the presumed SbF_5 by-product was not detected due to broadening of the ^{19}F signals by quadrupolar $^{121/123}Sb$ isotopes and low concentration.[56] We propose a mechanism whereby the electrophilic carbene center abstracts a hydride

from the silane, with the resulting silylium cation (Scheme 5), abstracting a fluoride from the SbF_6 counteranion.[57]

Scheme 5. Reaction of 2 with Silane

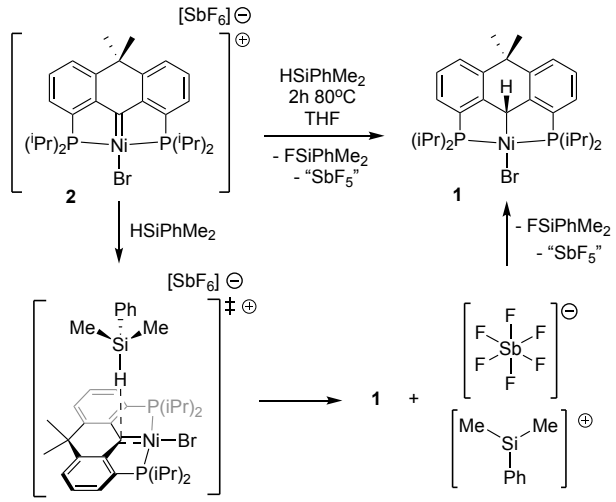

The apparent ability of **2** to generate solvated silylium cations *in situ* led us to probe the efficacy of **2** in the catalytic hydrodefluorination of α,α,α-trifluorotoluene. While nickel complexes are known to be active in the hydrodefluorination of aryl fluorides,[58] the catalyst landscape for effecting this transformation on alkyl fluoride substrates is dominated by highly electrophilic main group species,[59-63] with few examples of nickel based catalysts.[64, 65] Treatment of **2** in neat α,α,α-trifluorotoluene with $K[B(C_6F_5)]$ effectively exchanges the $[SbF_6]^-$ counterion with the less reactive $[B(C_6F_5)_4]^-$ anion, resulting in no changes in the $^{31}P\{^1H\}$ NMR spectrum. Treatment of this solution with excess $HSiEt_3$ resulted in no reaction at room temperature; however, heating the mixture to 80°C for 1h led to the formation of 35 equivalents of $FSiEt_3$ per **2** by $^{19}F\{^1H\}$ NMR (Fig. S3) spectroscopy with the loss of peaks in the $^{31}P\{^1H\}$ NMR spectra and the concomitant formation of a black precipitate. Further heating gave no additional $FSiEt_3$ formation. ^1H NMR spectroscopy (Fig. S4) and GC/MS (Fig. S5) analysis of the reaction mixture confirmed the formation of toluene, suggesting F-Si bond formation is not simply due to activation of the counter ion. While the catalytic performance is admittedly modest considering the activity observed silylium carborane catalysts,[60, 61] it compares favorably to silylium[59] (TON = 60) and phosphonium[62] (TON = 33) catalysts containing the tetrakis(pentafluorophenyl)borate counterion and the reported $NiCl_2/LiHBEt_3$ system[64] (TON = 2.5).

Given the reactivity of **2** towards the modestly polar Si-H bond of silanes, we sought to explore the reactivity of **2** towards the oppositely polarized N-H bond of ammonia, as activation of the N-H bond is a key step in the conversion of ammonia to value added products through C-N bond forming reactions.[66, 67] Since ammonia typically undergoes Werner-type coordination with transition metals rather than oxidative addition, this is a challenging bond activation. While oxidative addition of ammonia has been observed in both transition metal[68-70] and main group systems,[71-74] other modes of activation have been explored to circumvent the need for oxidative addition.[75] Chief among these are transition metal induced homolytic bond weakening of ammonia followed by H atom elimination or abstraction,[76-78] heterolytic bond weakening by electropositive metal centers followed by deprotonation by a strong external base,[79-81] ligand metathesis,[82-90] and metal-ligand cooperative N-H bond activation.[4, 12, 91-95]

While a variety of systems have shown to be competent for the metal ligand cooperative activation of ammonia, including **I**,[12] in all cases the systems operate by the same process, formal deprotonation of ammonia by a highly reactive, basic, ligand functionality, such as dearomatized pyridine or a late transition metal imide or carbene, such as in **I**.[12] In contrast, the industrial synthesis of HCN from ammonia and methane *via* the Degussa BMA process is proposed to proceed through the activation of ammonia at an electrophilic methylidene fragment on a platinum surface to form a C-N bond.[96] Given the electrophilic nature of the carbene fragment of **2**, any ammonia activation is unlikely to be effected in the same manner as **I**, and may give insight into the mechanism of C-N bond forming reactions at carbene centers.

Reaction of **2** with one atmosphere of ammonia (Scheme 6) in solution consistently results in three diamagnetic phosphorus containing products, in varying relative amounts depending on temperature, initial concentration of **2** and even the shape of

Scheme 6. Reactions of **2** with Ammonia and PMe_3

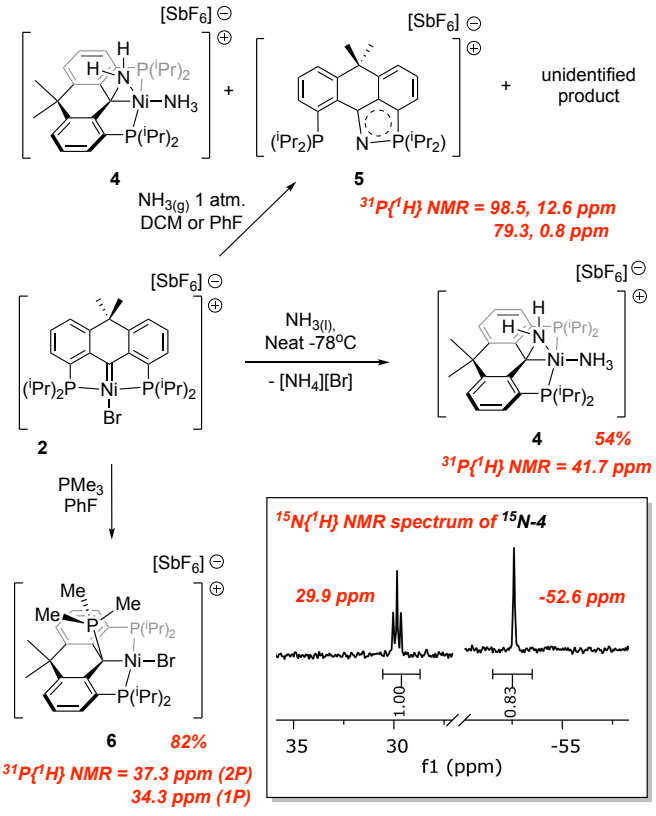

the reaction vessel (see Fig. S6 for a representative spectrum). Treatment of this mixture with excess ammonia, vacuum or

heat does not change the product distribution and there is no evidence of interconversion of the three products. Fractional recrystallization of the reaction mixture allowed for the identification of two of the three products *via* single crystal X-ray diffraction studies. The nickel containing product **4** (Fig. 5) was associated with the ^{31}P NMR signal at 41.7 ppm, and could be prepared selectively in 54% isolated yield by treating **2** with neat ammonia (Scheme 6). The other identified product **5** is consistent with the ^{31}P NMR pattern found for the unsymmetrical phosphorus containing products observed in the solution reaction and is the C_1 symmetric P-N heterocyclic compound **5** (Fig. S7). The third, unidentified product is likely closely related to **5** as both show two inequivalent phosphorus nuclei, one downfield and consistent with P(V) (98.5 ppm and 79.3 ppm), one upfield and indicative of P(III) (12.6 and 0.8 ppm), and small $J_{P\text{-}P}$ (16 and 29 Hz) coupling constants.[97] Given that **4** could be prepared selectively and that the by-products are the result of demetallation, we did not pursue absolute spectral assignment and full characterization of **5** or the other species.

Complex **4**, which corresponds to a singlet at 41.7 ppm in the ^{31}P{^{1}H} spectrum (THF-d^8), is the product of ammonia activation and C-N bond formation at the carbene center, as evidenced by the short C1-N1 contact of 1.440(4) Å (Fig. 5). It

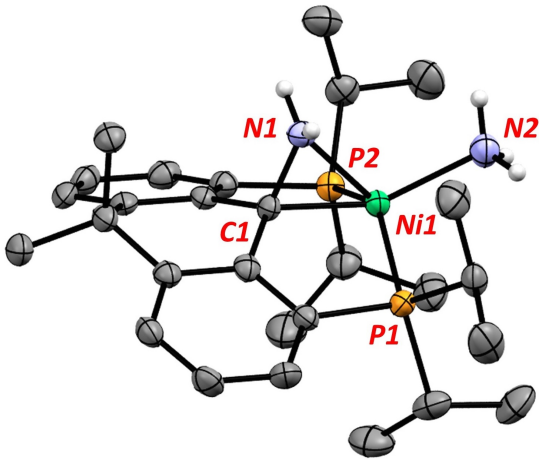

Figure 5. ORTEP diagram for complex 4. Thermal ellipsoids are shown at the 50% probability level. Hydrogen atoms and counter anion are omitted for clarity. Select bond lengths (Å) and angles (degrees) for **4**: Ni1-N2 2.013(3), Ni1-N1 2.050(3), Ni1-C1 1.926(3), N1-C1 1.440(4), C1-Ni1-N2 151.2(1), Ni1-C1-N1 73.5(2), C1-N1-Ni1 64.2(2), C1-Ni1-N1 42.3(1), N2-Ni1-N1 108.89. P1-N1 1.666(4), N1-C1 1.313(6), C1-C2 1.482(6), C2-C9 1.401(6), C9-P1 1.789(4).

is best described as a protonated metalloaziridine (sum ∠C1-N1-Ni1= 180.0(3)°). The signals for the NH_2 (3.79 ppm) and NH_3 (1.53 ppm) in the ^{1}H NMR spectrum split into doublets when **4** is prepared with ^{15}NH_3 (Fig. S9). The ^{15}N resonances (inset, Scheme 6) for the *N*H_2 (triplet, 29.9 ppm, $^3J_{N\text{-}P}$ = 9.8Hz) and *N*H_3 (singlet, -52.6 ppm) were assigned by ^{1}H-^{15}N correlation spectroscopy, and show that only the NH_2 moiety couples to the ^{31}P nuclei; a corresponding doublet splitting is observed in the ^{31}P{^{1}H} NMR spectrum (Fig. S9). The absence of $^2J_{N\text{-}N}$ coupling as well as the lack of coupling between the Ni-ammonia fragment and the ligand phosphines suggests ^2J coupling is not observable in this system.

The path to ammonia activation by **2** likely involves initial coordination of NH_3 to the electrophilic carbene carbon, but attempts to detect intermediates by following the reaction at low temperatures were not successful; product formation is very rapid even under these conditions. As a model reaction, **2** was treated with isoelectronic, proton free, PMe_3 and as shown in Scheme 6, leads to immediate formation of compound **6**. The ^{31}P{^{1}H} NMR spectrum shows two singlets at 37.3 and 34.3 ppm, integrating 2:1, consistent with incorporation of one PMe_3 fragment. The ^{13}C{^{1}H} NMR spectrum reveals a dramatic upfield shift of the Ni-C resonance from 250.9 ppm to a multiplet at 47.27 – 44.57 ppm, consistent with carbon centered phosphorus binding. This binding mode was unambiguously confirmed by a solid-state structure (Fig. 6) showing ylide formation. Notably, the bond length of the Ni-C bond has increased to 1.981(7) Å, a change of 0.107 Å, suggesting the PMe_3 lone pair has occupied an orbital with Ni-C antibonding character, consistent with the previously discussed electronic structure of **2**. Ylide formation is in direct contrast with the reactivity of **II**, which undergoes exchange of the neutral L-type ligand at Ni with PMe_3, and not carbene centered reactivity; however, ylide formation consistent with numerous examples of group 9 and 10 carbene complexes containing electrophilic carbene centers.[20, 27, 42, 46, 98, 99]

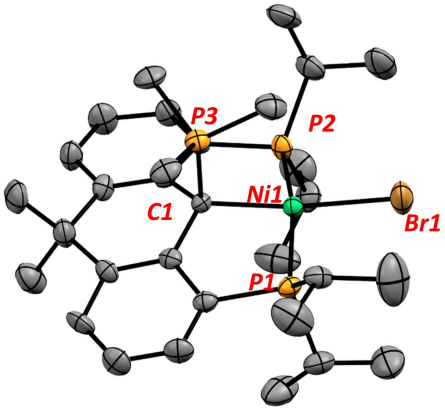

Figure 6. ORTEP diagram for complex 6. Thermal ellipsoids are shown at the 50% probability level. Hydrogen atoms and counter anions are omitted for clarity. Select bond lengths (Å) and angles (degrees) for 4: Ni1-C1 1.981(7), Ni1-Br1 2.340(1), C1-P3 1.854(8), Ni1-C1-P3 98.5(3),C1-Ni1-Br1 172.0(2), P1-Ni1-P2 162.36(9).

Although the intimate details concerning the mechanism of formation of **4** are opaque, based on the PMe_3 chemistry, the first step is undoubtedly coordination of NH_3 to the carbene carbon (Scheme 7). Since a cleaner reaction is observed when a large excess of ammonia is present, the path to **4** likely involves deprotonation of this species by a second equivalent of NH_3, elimination of [NH_4][Br] and trapping of the resulting coordinatively unsaturated Ni centre with a third equivalent of NH_3. With lower concentrations of ammonia, inefficient trapping and/or side reactions lead to side products **5**. The elimination of ammonium as the bromide salt suggests an

inner sphere salt elimination, probably assisted by hydrogen bonding from excess ammonia present.

Coordination of ammonia to an electrophilic carbene followed by deprotonation as shown in Scheme 7 is a distinctive mode of ammonia activation. Typically deprotonation of coordinated ammonia requires a stronger alkali metal alkoxo or amido base,[79, 80] suggesting significant activation of the ammonia N-H bonds in unobserved **V**. Furthermore, this mode of ligand centered ammonia activation is unusual in that known metal-ligand cooperative ammonia activation proceeds by formal ammonia deprotonation by a basic ligand functionality,[12, 91-94] and the metathesis is normally observed in multi-metallic compounds containing platinum group metals,[83, 84, 88, 90] or species containing reactive metal-carbon or hydride fragments.[85-87, 89]

Scheme 7. Plausible path of formation for **4** from **2** and NH_3.

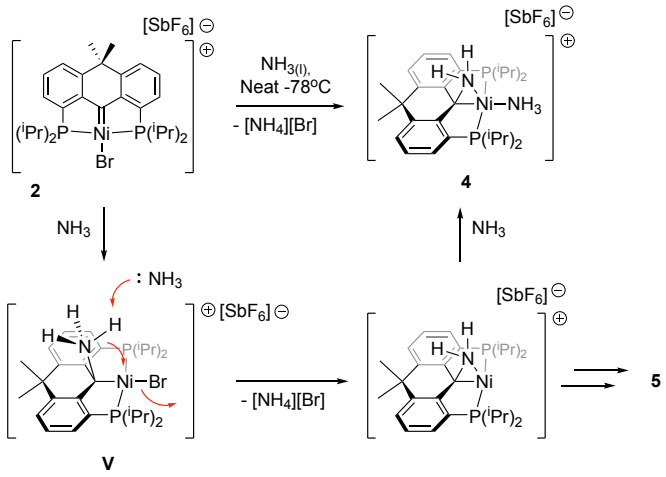

Conclusions

This work demonstrates the synthesis of a novel electrophilic Ni carbene complex **2** supported by a rigid pincer ligand framework, with an electronic structure and reactivity profile distinct from that of previously reported nickel carbenes. The carbene ligand was shown to be both the locus of reduction *via* electron transfer to yield radical carbene $\mathbf{2}_{red}$ and oxidation *via* group transfer. $\mathbf{2}_{red}$ is remarkable for its chemical stability, exhibiting virtually no reactivity towards substrates readily activated by its one electron oxidation or reduction product, while the group transfer chemistry could be of interest in the development of organic oxidations *via* carbene intermediates.[100] Electrophilic complex **2** shows ligand centred modes reactivity with both Si-H bonds and NH_3, contrasting with known nucleophilic analogue **I**. Further, the rigid chelate structure allowed for the first study of ammonia activation by a late metal electrophilic carbene complex, demonstrating the viability of these species in direct C-N bond forming reactions between ammonia and hydrocarbons. N-H bond cleavage proceeds by an unusual mechanism, suggesting these species may be capable of metal-ligand cooperative type reactivity in some cases, though a ligand-only process cannot be discounted.

References and Notes

‡ No corresponding peaks for disilane formation were observed. This can be explained either by obfuscation of the peaks by the excess silane, or by H-atom abstraction from the glass to regenerate the starting reagent being competitive to dimerization at the low concentrations of radicals.

1. J. P. Collman and W. R. Roper, *Adv. Organomet. Chem.*, 1968, **7**, 53-94.
2. J. Halpern, *Acc. Chem. Res.*, 1970, **3**, 386-392.
3. M. E. Thompson, S. M. Baxter, A. R. Bulls, B. J. Burger, M. C. Nolan, B. D. Santarsiero, W. P. Schaefer and J. E. Bercaw, *J. Am. Chem. Soc.*, 1987, **109**, 203-219.
4. J. R. Khusnutdinova and D. Milstein, *Angew. Chem. Int. Ed.*, 2015, **54**, 12236-12273.
5. D. Gelman and S. Musa, *ACS Catal.*, 2012, **2**, 2456-2466.
6. D. Gelman and R. Romm, *Top. Organomet. Chem.*, 2013, **40**.
7. J. I. van der Vlugt, *Eur. J. Inorg. Chem.*, 2012, **2012**, 363-375.
8. H. Grutzmacher, *Angew. Chem. Int. Ed.*, 2008, **47**, 1814-1818.
9. C. Gunanathan and D. Milstein, *Acc. Chem. Res.*, 2011, **44**, 588-602.
10. K. S. Feichtner and V. H. Gessner, *Chem. Commun.*, 2018, **54**, 6540-6553.
11. P. Cui and V. M. Iluc, in *Pincer Compounds*, ed. D. Morales-Morales, Elsevier, 2018, pp. 359-381.
12. D. V. Gutsulyak, W. E. Piers, J. Borau-Garcia and M. Parvez, *J. Am. Chem. Soc.*, 2013, **135**, 11776-11779.
13. E. A. LaPierre, W. E. Piers and C. Gendy, *Organometallics*, 2018, DOI: 10.1021/acs.organomet.8b00440.
14. E. A. LaPierre, W. E. Piers, D. M. Spasyuk and D. W. Bi, *Chem. Commun.*, 2016, **52**, 1361-1364.
15. J. Borau-Garcia, D. V. Gutsulyak, R. J. Burford and W. E. Piers, *Dalton Trans.*, 2015, **44**, 12082-12085.
16. C. C. Comanescu and V. M. Iluc, *Organometallics*, 2015, **34**, 4684-4692.
17. C. C. Comanescu and V. M. Iluc, *Polyhedron*, 2018, **143**, 176-183.
18. C. C. Comanescu and V. M. Iluc, *Organometallics*, 2014, **33**, 6059-6064.
19. C. C. Comanescu and V. M. Iluc, *Chem. Commun.*, 2016, **52**, 9048-9051.
20. P. Cui and V. M. Iluc, *Chem. Sci.*, 2015, **6**, 7343-7354.
21. A. Furstner and P. W. Davies, *Angew. Chem. Int. Ed.*, 2007, **46**, 3410-3449.
22. Q. Xiao, Y. Zhang and J. Wang, *Acc. Chem. Res.*, 2013, **46**, 236-247.
23. M. T. Whited and R. H. Grubbs, *Acc. Chem. Res.*, 2009, **42**, 1607-1616.
24. M. T. Whited and R. H. Grubbs, *J. Am. Chem. Soc.*, 2008, **130**, 5874-5875.
25. C. Yoo and Y. Lee, *Angew. Chem. Int. Ed.*, 2017, **56**, 9502-9506.
26. R. Peloso and E. Carmona, *Coord. Chem. Rev.*, 2018, **355**, 116-132.
27. J. Campos, R. Peloso and E. Carmona, *Angew. Chem. Int. Ed.*, 2012, **51**, 8255-8258.
28. V. M. Iluc and G. L. Hillhouse, *J. Am. Chem. Soc.*, 2014, **136**, 6479-6488.

29. M. Bröring, C. D. Brandt and S. Stellwag, *Chem. Commun.*, 2003, DOI: 10.1039/b307160j, 2344-2345.
30. W. Weng, C. H. Chen, B. M. Foxman and O. V. Ozerov, *Organometallics*, 2007, **26**, 3315-3320.
31. D. J. Mindiola and G. L. Hillhouse, *J. Am. Chem. Soc.*, 2002, **124**, 9976-9977.
32. C. C. Comanescu, M. Vyushkova and V. M. Iluc, *Chem. Sci.*, 2015, **6**, 4570-4579.
33. N. G. Connelly and W. E. Geiger, *Chem. Rev.*, 1996, **96**, 877-910.
34. F. H. Allen, O. Kennard, D. G. Watson, L. Brammer, A. G. Orpen and R. Taylor, *J. Chem. Soc., Perkin Trans. 2*, 1987, DOI: 10.1039/p298700000s1, S1.
35. L. E. Doyle, W. E. Piers and J. Borau-Garcia, *J. Am. Chem. Soc.*, 2015, **137**, 2187-2190.
36. N. D. Harrold, R. Waterman, G. L. Hillhouse and T. R. Cundari, *J. Am. Chem. Soc.*, 2009, **131**, 12872-12873.
37. D. J. Mindiola, R. Waterman, D. M. Jenkins and G. L. Hillhouse, *Inorg. Chim. Acta*, 2003, **345**, 299-308.
38. P. E. Rothstein, C. C. Comanescu and V. M. Iluc, *Chem. Eur. J.*, 2017, **23**, 16948-16952.
39. L. Y. Fan, F. F. Gao, W. H. Jiang, M. Z. Deng and C. T. Qian, *Org. Biomol. Chem.*, 2008, **6**, 2133-2137.
40. E. A. LaPierre, M. L. Clapson, W. E. Piers, L. Maron, D. M. Spasyuk and C. Gendy, *Inorg. Chem.*, 2018, **57**, 495-506.
41. R. Waterman and G. L. Hillhouse, *J. Am. Chem. Soc.*, 2003, **125**, 13350-13351.
42. M. D. Fryzuk, X. L. Gao, K. Joshi, P. A. Macneil and R. L. Massey, *J. Am. Chem. Soc.*, 1993, **115**, 10581-10590.
43. M. D. Fryzuk, P. A. Macneil and S. J. Rettig, *J. Am. Chem. Soc.*, 1985, **107**, 6708-6710.
44. J. Campos, J. Lopez Serrano, E. Alvarez and E. Carmona, *J. Am. Chem. Soc.*, 2012, **134**, 7165-7175.
45. J. Campos and E. Carmona, *Organometallics*, 2014, **34**, 2212-2221.
46. J. Campos, R. Peloso, M. Brookhart and E. Carmona, *Organometallics*, 2013, **32**, 3423-3426.
47. D. P. Klein and R. G. Bergman, *J. Am. Chem. Soc.*, 1989, **111**, 3079-3080.
48. R. J. Burford, W. E. Piers and M. Parvez, *Organometallics*, 2012, **31**, 2949-2952.
49. N. M. Camasso and M. S. Sanford, *Science*, 2015, **347**, 1218-1220.
50. J. R. Bour, N. M. Camasso and M. S. Sanford, *J. Am. Chem. Soc.*, 2015, **137**, 8034-8037.
51. E. A. Meucci, N. M. Camasso and M. S. Sanford, *Organometallics*, 2016, **36**, 247-250.
52. E. Chong, J. W. Kampf, A. Ariafard, A. J. Canty and M. S. Sanford, *J. Am. Chem. Soc.*, 2017, **139**, 6058-6061.
53. M. B. Watson, N. P. Rath and L. M. Mirica, *J. Am. Chem. Soc.*, 2017, **139**, 35-38.
54. G. E. Martinez, C. Ocampo, Y. J. Park and A. R. Fout, *J. Am. Chem. Soc.*, 2016, **138**, 4290-4293.
55. W. Liu, K. Welch, C. O. Trindle, M. Sabat, W. H. Myers and W. D. Harman, *Organometallics*, 2007, **26**, 2589-2597.
56. A. Bock, M. Dubois, P. Bonnet, A. Hamwi, D. Avignant, L. Moch and B. Morel, *J. Fluor. Chem.*, 2012, **134**, 24-28.
57. M. Brookhart, B. Grant and A. F. Volpe, *Organometallics*, 1992, **11**, 3920-3922.
58. M. K. Whittlesey and E. Peris, *ACS Catal.*, 2014, **4**, 3152-3159.
59. V. J. Scott, R. Çelenligil-Çetin and O. V. Ozerov, *J. Am. Chem. Soc.*, 2005, **127**, 2852-2853.
60. C. Douvris and O. V. Ozerov, *Science*, 2008, **321**, 1188.
61. C. Douvris, C. M. Nagaraja, C.-H. Chen, B. M. Foxman and O. V. Ozerov, *J. Am. Chem. Soc.*, 2010, **132**, 4946-4953.
62. C. B. Caputo, L. J. Hounjet, R. Dobrovetsky and D. W. Stephan, *Science*, 2013, **341**, 1374.
63. T. Stahl, H. F. T. Klare and M. Oestreich, *ACS Catal.*, 2013, **3**, 1578-1587.
64. J. Wu and S. Cao, *ChemCatChem*, 2011, **3**, 1582-1586.
65. J. Wenz, C. A. Rettenmeier, H. Wadepohl and L. H. Gade, *Chem. Comm.*, 2016, **52**, 202-205.
66. J. I. van der Vlugt, *Chem. Soc. Rev.*, 2010, **39**, 2302-2322.
67. J. L. Klinkenberg and J. F. Hartwig, *Angew. Chem. In.t Ed.*, 2011, **50**, 86-95.
68. J. Zhao, A. S. Goldman and J. F. Hartwig, *Science*, 2005, **307**, 1080-1082.
69. E. Morgan, D. F. MacLean, R. McDonald and L. Turculet, *J. Am. Chem. Soc.*, 2009, **131**, 14234-14236.
70. A. L. Casalnuovo, J. C. Calabrese and D. Milstein, *Inorg. Chem.*, 1987, **26**, 971-973.
71. G. D. Frey, V. Lavallo, B. Donnadieu, W. W. Schoeller and G. Bertrand, *Science*, 2007, **316**, 439-441.
72. A. Jana, C. Schulzke and H. W. Roesky, *J. Am. Chem. Soc.*, 2009, **131**, 4600-4601.
73. T. P. Robinson, D. M. De Rosa, S. Aldridge and J. M. Goicoechea, *Angew. Chem. Int. Ed.*, 2015, **54**, 13758-13763.
74. S. M. McCarthy, Y. C. Lin, D. Devarajan, J. W. Chang, H. P. Yennawar, R. M. Rioux, D. H. Ess and A. T. Radosevich, *J. Am. Chem. Soc.*, 2014, **136**, 4640-4650.
75. J. Hoover, *Science*, 2016, **354**, 707-708.
76. M. J. Bezdek, S. Guo and P. J. Chirik, *Science*, 2016, **354**, 730-733.
77. G. W. Margulieux, M. J. Bezdek, Z. R. Turner and P. J. Chirik, *J. Am. Chem. Soc.*, 2017, **139**, 6110-6113.
78. P. Bhattacharya, Z. M. Heiden, E. S. Wiedner, S. Raugei, N. A. Piro, W. S. Kassel, R. M. Bullock and M. T. Mock, *J. Am. Chem. Soc.*, 2017, **139**, 2916-2919.
79. J. L. Klinkenberg and J. F. Hartwig, *J. Am. Chem. Soc.*, 2010, **132**, 11830-11833.
80. D. J. Fox and R. G. Bergman, *Organometallics*, 2004, **23**, 1656-1670.
81. G. Bai, H. W. Roesky, H.-G. Schmidt and M. Noltemeyer, *Organometallics*, 2001, **20**, 2962-2965.
82. C. Stanciu, S. S. Hino, M. Stender, A. F. Richards, M. M. Olmstead and P. P. Power, *Inorg. Chem.*, 2005, **44**, 2774-2780.
83. J. J. Li, W. Li, A. J. James, T. Holbert, T. P. Sharp and P. R. Sharp, *Inorg. Chem.*, 1999, **38**, 1563-1572.
84. I. Mena, M. A. Casado, P. Garcia-Orduna, V. Polo, F. J. Lahoz, A. Fazal and L. A. Oro, *Angew. Chem. Int. Ed.*, 2011, **50**, 11735-11738.
85. C. Ni, H. Lei and P. P. Power, *Organometallics*, 2010, **29**, 1988-1991.
86. Y. Peng, B. D. Ellis, X. Wang and P. P. Power, *J. Am. Chem. Soc.*, 2008, **130**, 12268-12269.
87. Y. Peng, J. D. Guo, B. D. Ellis, Z. Zhu, J. C. Fettinger, S. Nagase and P. P. Power, *J. Am. Chem. Soc.*, 2009, **131**, 16272-16282.

88. M. Juribasic Kulcsar, I. Halasz, A. Budimir, K. Uzarevic, S. Lukin, A. Monas, F. Emmerling, J. Plavec and M. Curic, *Inorg. Chem.*, 2017, **56**, 5342-5351.
89. G. L. Hillhouse and J. E. Bercaw, *J. Am. Chem. Soc.*, 1984, **106**, 5472-5478.
90. Y. Nakajima, H. Kameo and H. Suzuki, *Angew. Chem. Int. Ed.*, 2006, **45**, 950-952.
91. E. Khaskin, M. A. Iron, L. J. Shimon, J. Zhang and D. Milstein, *J. Am. Chem. Soc.*, 2010, **132**, 8542-8543.
92. Y. H. Chang, Y. Nakajima, H. Tanaka, K. Yoshizawa and F. Ozawa, *J. Am. Chem. Soc.*, 2013, **135**, 11791-11794.
93. R. M. Brown, J. Borau Garcia, J. Valjus, C. J. Roberts, H. M. Tuononen, M. Parvez and R. Roesler, *Angew. Chem. Int. Ed.*, 2015, **54**, 6274-6277.
94. T. Kimura, N. Koiso, K. Ishiwata, S. Kuwata and T. Ikariya, *J. Am. Chem. Soc.*, 2011, **133**, 8880-8883.
95. A. Jana, I. Objartel, H. W. Roesky and D. Stalke, *Inorg. Chem.*, 2009, **48**, 798-800.
96. M. Aschi, M. Bronstrup, M. Diefenbach, J. N. Harvey, D. Schroder and H. Schwarz, *Angew. Chem. Int. Ed.*, 1998, **37**, 829-832.
97. M. Doskocz, B. Malinowska, P. Młynarz, B. Lejczak and P. Kafarski, *Tet. Lett.*, 2010, **51**, 3406-3411.
98. S. Martinez-Salvador, B. Menjon, J. Fornies, A. Martin and I. Uson, *Angew. Chem. Int. Ed.*, 2010, **49**, 4286-4289.
99. S. Sung, T. Joachim, T. Krämer and R. D. Young, *Organometallics*, 2017, **36**, 3117-3124.
100. R. Dorel and A. M. Echavarren, *Chem. Rev.*, 2015, **115**, 9028-9072.

Supporting Information

Redox–state Dependent Activation of Silanes and Ammonia with Reverse Polarity ($PC_{carbene}P$)Ni Complexes: Electrophilic vs. Nucleophilic Carbenes

Etienne A. LaPierre, Warren E. Piers*, Chris Gendy

University of Calgary, Department of Chemistry, 2500 University Drive N.W., Calgary, Alberta, Canada, T2N 1N4.

Contents

Experimental Details

General Considerations. Storage and manipulation of all compounds were performed under an argon atmosphere either in a IT glove box or using a double manifold high vacuum line using standard techniques. Passage of argon through an OxisorBW scrubber (Matheson Gas Products) removed any residual oxygen and moisture. Toluene, hexanes, pentane and tetrahydrofuran were dried and purified using a Grubbs/Dow solvent purification system and stored in 500 mL thick-walled glass vessels over sodium/benzophenone ketal or CaH_2, and distilled under reduced pressure. C_6D_6 and THF-d_8 were dried over sodium/benzophenone ketal, CD_2Cl_2 was dried over CaH_2. All dried solvents were degassed and vacuum distilled prior to use. Anhydrous ammonia was purchased from Air Liquide and purified by condensation on sodium leading to an amber electrolyte. All other reagents were purchased from Sigma-Aldrich and used as received. ^{1}H and ^{13}C NMR spectrometry chemical shifts were referenced to residual proteo-solvent resonances and naturally abundant ^{13}C resonances for all deuterated solvents. ^{15}N NMR experiments were referenced to $NH_{3(l)}$ at 0 ppm. All other heteronuclear NMR spectrum were referenced externally to IUPAC standards. Chemical shift assignments are based on ^{1} H, $^{13}C\{^{1}H\}$, $^{31}P\{^{1}H\}$, $^{19}F\{^{1}H\}$, ^{1}H- ^{13}C-HSQC and ^{1} H- ^{13}C-HMBC NMR experiments performed on Bruker Ultrashield 400, Ascend-500 or Avance-600 MHz spectrometers. **1**,[1] PhINTs[2] and $ONMePh_2$[3] were prepared per literature procedures. Electrochemical measurements were performed using a CH instruments electrochemical workstation in a drybox under an atmosphere of argon. GC/MS were performed using an Agilent 7890B GC equipped with an Agilent 5977A MSD. All elemental analyses were obtained by the Instrumentation Facility of the Department of Chemistry, University of Calgary. Diffraction patterns were collected with Cu Kα radiation on a Bruker Smart diffractometer equipped with Apex II detector, fixed-CHI goniometer, and sealed-tube (Cu) source or with Mo Kα radiation on a Nonius Kappa CCD diffractometer.

Synthesis of Complex 2

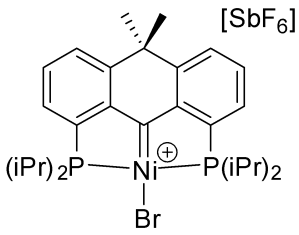

A solution of 200 mg (0.346 mmol) of **1** in 4 mL of DCM was prepared in a 20 mL scintillation vial. To the solution was added 165 mg (0.346 mmol) of $[CPh_3][SbF_6]$, resulting in the immediate color change to dark green. The solution was allowed to stand overnight and then layered with 15 mL *n*-pentane and cooled to -30 ^oC for 2 days. The resulting green-blue needles were separated from the mother liquor, dried *in vacuo*, and washed with 2x10 mL *n*-pentane to yield the title compound as an analytically pure crystalline solid. Crystals grown in this fashion were suitable for single crystal X-ray diffraction studies.

Yield: 270 mg, 0.332 mmol, 96%

^{31}P NMR (203 MHz, Methylene Chloride-d_2) δ 71.85.

^1H NMR (500 MHz, Methylene Chloride-d_2) δ 8.63 – 8.29 (m, Ar-**H**, 2H), 7.99 (dt, *J* = 7.9, 1.1 Hz, Ar-**H**, 2H), 7.96 – 7.81 (m, Ar-**H**, 2H), 3.16 (m, P-C**H**$(CH_3)_2$, 4H), 1.78 (s, C(C**H**$_3)_2$, 6H), 1.43 (m, P-CH(C**H**$_3)_2$, 24H).

^{13}C NMR (126 MHz, Methylene Chloride-d_2) δ 250.79 (t, *J* = 9.6 Hz, Ni=**C**), 154.05 (t, *J* = 19.1 Hz, $\mathbf{C_{Aryl}}$), 151.14 (t, *J* = 6.2 Hz, $\mathbf{C_{Aryl}}$), 141.22 (t, *J* = 16.1 Hz, $\mathbf{C_{Aryl}}$), 139.83 (t, *J* = 3.3 Hz, $\mathbf{C_{Aryl}}$), 132.52 ($\mathbf{C_{Aryl}}$), 132.40 ($\mathbf{C_{Aryl}}$), 42.37 (**C**$(CH_3)_2$), 28.82 (C(**C**$H_3)_2$), 25.22 (t, *J* = 12.2 Hz, P-**C**$H(CH_3)_2$), 18.21 (P-CH(**C**$H_3)_2$), 17.45, (P-CH(**C**$H_3)_2$) .

Elemental Analysis: Calcd (%): C 41.37; H 4.96. Found (%): C 41.43; H 5.07

Synthesis of Complex 2_{red}

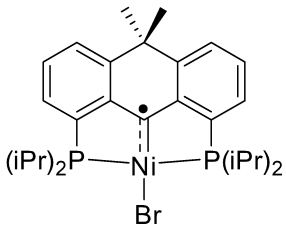

To 3 mL of a THF solution of 100 mg (0.123 mmol) of **2** was added 25 mg (0.129 mmol, 1.05 eq) of solid cobaltocene. An immediate color change from blue-green to blue-red was noted. The solvent was removed *in vacuo* and the dark blue residue was extracted with 5 mL n-pentane from the yellow cobaltocenium salt. The suspension was filtered through a 0.2 μm PTFE syringe filter, and cooled to -30 ^oC to yield analytically pure **3** as dichroic blue-red X-ray quality crystals.

Yield: 36 mg, 0.062 mmol, 51%

μ_{eff}=1.76 μ_B (Evan's Method)

Elemental Analysis: Calcd (%): C 58.27; H 6.99. Found (%): C 58.26; H 6.86.

Synthesis of 3_O

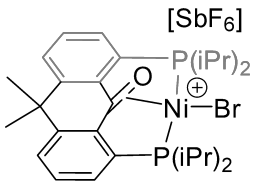

To a cold (-30 °C) 4 mL of a DCM solution containing **2** (50 mg, 0.061 mmol) was added 13mg (0.065 mmol, 1.05 eq.) of $ONMePh_2$ as a solid. The solution immediately became dark brown. The solution was layered with 15 mL n-pentane, and cooled to -30°C for two days. The mother liquor was separated by decantation. The brown residue was dissolved in minimal DCM and layered with 15 mL n-pentane and cooled to -30 °C for a further 2 days. The resulting brown residue was isolated by decantation and dried under vacuum. X-ray quality crystals were grown by vapor diffusion of n-pentane to a saturated fluorobenzene (~4 mg/mL) solution at ambient temperature.

IR ν=1571 cm^{-1}

Yield 39 mg, 0.047 mmol, 76%

^{31}P NMR (203 MHz, Methylene Chloride-d_2) δ 30.94.

^{1}H NMR (500 MHz, Methylene Chloride-d_2) δ 8.11 – 7.85 (m, 4H, Ar-**H**), 7.53 (m, 2H), 2.72 – 2.62 (m, P-C**H**$(CH_3)_2$, 2H), 2.49 (m, P-C**H**$(CH_3)_2$, 2H), 2.03 (s, C(C**H**$_3)_2$, 3H), 1.72 (dd, J = 8.2 Hz, P-CH(C**H**$_3)_2$, 6H), 1.63 (s, C(C**H**$_3)_2$, P-CH(C**H**$_3)_2$, 6H), 1.28 (m, P-CH(C**H**$_3)_2$, 12H).

^{13}C NMR (126 MHz, Methylene Chloride-d_2) δ 182.84 (**C**=O), 152.59 (**C**$_{Aryl}$), 138.19 (**C**$_{Aryl}$), 137.31 (t, J = 3.4 Hz, **C**$_{Aryl}$), 131.81 (**C**$_{Aryl}$), 130.92 (**C**$_{Aryl}$). 127.18 (t, J = 13.9 Hz, **C**$_{Aryl}$), 40.99 (**C**$(CH_3)_2$), 34.61 (C(**C**$H_3)_2$), 28.49 (C(**C**$H_3)_2$), 26.74 (t, J = 10.2 Hz, P-**C**H$(CH_3)_2$), 24.84 (t, J = 12.1 Hz, P-**C**H$(CH_3)_2$), 19.79 (P-CH(**C**$H_3)_2$), 18.83 (P-CH(**C**$H_3)_2$), 18.29 (P-CH(**C**$H_3)_2$), 17.15 (P-CH(**C**$H_3)_2$).

Elemental Analysis: Calcd (%): C 40.57; H 4.86. Found (%): C 40.85; H 5.04; N 0.04.

Synthesis of 3_{NTs}

To a cold (-30 °C) 4 mL of a DCM solution containing **2** (60 mg, 0.074 mmol) was added 28 mg (0.078 mmol, 1.05 eq.) of $ONMePh_2$ as a solid. The solution immediately became dark brown.

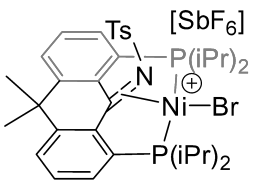

The solution was layered with 15 mL n-pentane, and cooled to -30°C for two days. The mother liquor was separated by decantation. The brown residue was dissolved in minimal THF and layered with 15 mL n-pentane and cooled to -30 °C for a further 2 days. The resulting brown residue was isolated by decantation and dried under vacuum. X-ray quality crystals were grown by vapor diffusion of n-pentane in to a saturated fluorobenzene (~4 mg/mL) solution at ambient temperature.

Yield:45 mg, 0.0458 mmol, 62%

IR ν=1595 cm^{-1}

^{31}P NMR (243 MHz, Methylene Chloride-d_2) δ 40.47.

^{1}H NMR (600 MHz, Methylene Chloride-d_2) δ 7.97 – 7.86 (m, Ar-**H**(ligand), 4H), 7.53 (m, Ar-**H**(ligand), 2H), 7.42 (d, J = 8.1 Hz, Ar-**H**, Ts, 2H), 7.24 (d, J = 8.1 Hz, Ar-**H**, Ts, 2H), 2.95 – 2.81 (m, P-C**H**$(CH_3)_2$, 4H), 2.36 (s, Ts C$\mathbf{H_3}$, 3H), 1.94 (s, C(C$\mathbf{H}_3)_2$, 3H), 1.82 – 1.68 (m, 6H), 1.59 (dd, J = 7.7 Hz, P-CH(C$\mathbf{H}_3)_2$ 6H), 1.36 (s, C(C$\mathbf{H}_3)_2$, 3H), 1.32 (dd, J = 8.1 Hz, P-CH(C$\mathbf{H}_3)_2$, 6H), 1.23 (dd, J = 7.5 Hz, P-CH(C$\mathbf{H}_3)_2$, 6H).

^{13}C NMR (151 MHz, Methylene Chloride-d_2) δ 149.27 (t, J = 4.2 Hz, $\mathbf{C_{Aryl}}$), 147.04 ($\mathbf{C_{Aryl}}$), 139.91 (**C**=N), 138.45 (t, J = 6.6 Hz, $\mathbf{C_{Aryl}}$), 136.16 ($\mathbf{C_{Aryl}}$), 135.18 (t, J = 3.4 Hz, $\mathbf{C_{Aryl}}$), 131.50 ($\mathbf{C_{Aryl}}$), 130.72 ($\mathbf{C_{Aryl}}$), 130.27 ($\mathbf{C_{Aryl}}$), 128.74 (t, J = 14.8 Hz, $\mathbf{C_{Aryl}}$), 127.61 ($\mathbf{C_{Aryl}}$), 41.25 (**C**$(CH_3)_2$), 35.84 (C(**C**$H_3)_2$), 28.79 (m, 2C, P-**C**$H(CH_3)_2$, 4.6 Hz), 28.07 (C(**C**$H_3)_2$), 21.84 (NTs **C**H_3), 20.37 (P-CH(**C**$H_3)_2$), 19.45 (P-CH(**C**$H_3)_2$), 19.39 (P-CH(**C**$H_3)_2$), 18.64 (P-CH(**C**$H_3)_2$).

Elemental Analysis: Calcd (%): C 42.80; H 4.82; N 1.43. Found (%): C 42.93; H 4.61; N 1.71.

Synthesis of Complex 4

To a 5 mL thick walled glass vessel containing fine ground **2** (50 mg, 0.061 mmol), was condensed 1.5 mL of freshly distilled liquid ammonia at -78°C. An immediate color change to red-purple was noted. The ammonia was removed *in vacuo*. The residue was extracted with 5 mL fluorobenzene and the resulting solution was filtered through a 0.2 μm PTFE syringe filter to remove a white precipitate. The solution was then layered with n-pentane to yield fuchsia

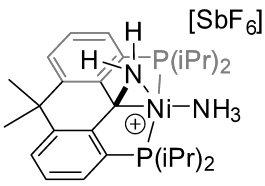

crystals of the title compound. Crystals suitable for X-ray diffraction were grown from 1:3 DCM/pentane at -30 ^{o}C.

Yield: 27 mg, 0.035 mmol, 58%

^{15}N NMR (51 MHz, THF-d_8) δ 29.85 (t, J = 9.8 Hz, C-**N**H_2-Ni), -52.59(s, Ni-**N**H_3).

^{31}P NMR (203 MHz, THF-d_8) δ 41.56.

^{1}H NMR (500 MHz, THF-d_8) δ 7.65 (d, J = 7.7 Hz, Ar-**H**, 2H), 7.60 (m, Ar-**H**, 2H), 7.47 (t, J = 7.7 Hz, Ar-**H**, 2H), 3.79 (s, N**H$_2$**, 2H), 2.95 – 2.80 (m, P-C**H**$(CH_3)_2$, 2H), 2.45 – 2.30 (m, P-C**H**$(CH_3)_2$, 2H), 1.86 (s, C(C**H**$_3)_2$, 3H), 1.58 (s, C(C**H**$_3)_2$, 3H), 1.53 (t, J = 4.1 Hz, N**H$_3$**, 3H), 1.49 – 1.41 (m, P-CH(C**H**$_3)_2$, 12H), 1.28 (dd, J = 7.1 Hz, P-CH(C**H**$_3)_2$, 6H), 0.92 (dd, J = 7.3 Hz, P-CH(C**H**$_3)_2$, 6H).

^{13}C NMR (126 MHz, THF-d_8) δ 149.41 (t, J = 20.2 Hz, **C$_{Aryl}$**), 145.10 (t, J = 7.8 Hz, **C$_{Aryl}$**), 133.89 – 133.43 (m, **C$_{Aryl}$**), 128.73 (**C$_{Aryl}$**), 127.86 (**C$_{Aryl}$**), 125.66 (**C$_{Aryl}$**), 63.53 (br s, N-**C**-Ni), 39.02 (**C**$(CH_3)_2$), 34.18 (C(**C**$H_3)_2$), 25.91 (t, (P-**C**$H(CH_3)_2$, J = 6.1 Hz), 24.50 (C(**C**$H_3)_2$), 18.50 (t, P-CH(**C**$H_3)_2$, J = 3.6 Hz), 18.40 (t, P-CH(**C**$H_3)_2$, J = 3.3 Hz), 17.72 (P-CH(**C**$H_3)_2$), 17.43 (t, P-CH(**C**$H_3)_2$, J = 3.5 Hz). Remaining peak for (P-**C**$H(CH_3)_2$) unresolved from solvent peak.

Elemental Analysis: Calcd (%): C 43.90; H 5.92; N 3.66. Found (%): C 44.39; H 5.68; N 3.32.

Synthesis of Complex 6

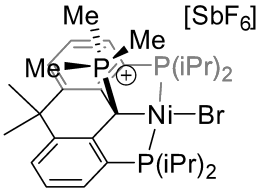

To 0.7 mL PhF solution containing 30 mg (0.037) of **2** in a 20 mL vial was added excess PMe_3 (1 drop, *via* Pasteur pipette). An immediate quenching of the intense blue-green color of **2**, leading to an orange-yellow solution. The solution was layered with 9 mL of *n*-pentane and cooled to -30^{o}C for two days. The resulting orange-yellow needles were separated from the mother liquor by decantation, washed with *n*-pentane and dried under vacuum. Crystals grown in this fashion were suitable for single crystal X-ray diffraction studies.

Yield: 27 mg, 0.0303 mmol, 82%

^{31}P NMR (203 MHz, Methylene Chloride-d_2) δ 37.28 (2P, Ligand), 34.29 (1P, **P**Me_3).

^{1}H NMR (500 MHz, Methylene Chloride-d_2) δ 7.75 (d, J = 7.1 Hz, Ar-**H**, 2H), 7.62 – 7.43 (m, Ar-**H**, 4H), 2.81 (m, P-C**H**$(CH_3)_2$, 2H), 2.76 – 2.67 (m, P-C**H**$(CH_3)_2$, 2H), 1.82 (s, C(C**H**$_3)_2$, 3H), 1.73 – 1.60 (m, P-CH(C**H**$_3)_2$, and P(C**H**$_3)_3$ 21H), 1.58 (s, C(C**H**$_3)_2$,3H), 1.30 (dd, J = 8.7, 7.1 Hz, P-CH(C**H**$_3)_2$, 6H), 1.15 (dd, J = 7.2 Hz, , P-CH(C**H**$_3)_2$, 6H).

^{13}C NMR (126 MHz, Methylene Chloride-d_2) δ 145.57 (td, J = 17.1, 6.2 Hz, **C$_{Aryl}$**), 144.54 (dd, J = 6.5 Hz, **C$_{Aryl}$**), 133.59 (m, **C$_{Aryl}$**), 130.76 (d, J = 5.0 Hz, **C$_{Aryl}$**), 130.00 (d, J = 4.4 Hz, **C$_{Aryl}$**), 128.94 – 128.25 (m, **C$_{Aryl}$**), 47.27 – 44.57 (m, P-**C**-Ni), 38.66 (d, J = 3.5 Hz, **C**$(CH_3)_2$), 35.13 (d, J = 6.7 Hz, C(**C**$H_3)_2$), 32.70 (d, J = 5.2 Hz, C(**C**$H_3)_2$), 28.04 (t, J = 12.0 Hz, P-**C**H$(CH_3)_2$), 25.85 (t, J = 11.1 Hz, P-**C**H$(CH_3)_2$), 19.76 (P-CH(**C**$H_3)_2$), 18.79 (P-CH(**C**$H_3)_2$), 18.73 (P-CH(**C**$H_3)_2$), 17.77 (P-CH(**C**$H_3)_2$), 12.47 (d, J = 51.0 Hz, P(**C**$H_3)_3$).

Elemental Analysis: Calcd (%): C 41.88; H 5.56. Found (%): C 41.53; H 5.76

Isolation of Crystals of 4 and 5

10 mg of **2** was dissolved in 0.5 mL DCM in a J-Young NMR tube. The solution was degassed by one freeze-pump-thaw cycle and placed under one atmosphere of $NH_{3(g)}$. The solution immediately changed color to deep red-purple. Volatiles were removed *in vacuo* and the residue was reconstituted in 1 mL DCM, filtered through a 0.2 μm PTFE syringe filter, layered with *n*-pentane and cooled to -30 ^{o}C for 2 days. The resulting fuchsia crystals (<1 mg) of **5** were manually separated from an orange oil, and the X-ray diffraction pattern collected. The oil was reconstituted in C_6D_6 and it was confirmed to be a mixture of **4$_a$** and an unidentified product. Vapor diffusion of pentane into this sample led to the precipitation of an orange oil. This orange oil was suspended in pentane and refrigerated at -30^{o}C for 6 weeks, leading to orange plate crystals (<1 mg).

Procedure for catalytic hydrodefluorination with 2

In a one dr. vial **2** 5.0 mg (0.0062 mmol) of **2** was dissolved in ca. 0.6 mL of α,α,α-trifluorotoluene and 6.0 mg (0.0083 mmol) of $K[B(C_6F_5)_4]$ was added. The mixture was agitated for 30 min and then filtered using a 0.2 μm PTFE syringe filter and the filtrate transferred to a J-Young NMR tube $^{31}P\{^1H\}$ NMR of this mixture showed 1 product identical to **2**, while $^{19}F\{^1H\}$ NMR showed the incorporation of $[B(C_6F_5)_4]^-$. To this solution was added 100 μL silane (0.652 mmol $HSiMe_2Ph$ or 0.626 mmol $HSiEt_3$). The reaction was allowed to stand for 30 min and then analysed by $^{19}F\{^1H\}$ and $^{31}P\{^1H\}$ spectrometry, showing no reaction. The reaction mixture was then heated to 80 ^oC for 30 min ($HSiMe_2Ph$) or 1 h ($HSiEt_3$), resulting in a color change to pale pink and the formation of a black precipitate (presumably Ni black). $^{19}F\{^1H\}$ and $^{11}B\{^1H\}$ NMR spectra suggest that the borate counter ion is still present, while the $^{31}P\{^1H\}$ NMR spectrum shows no trace of **1** or **2**. The tube was returned to the drybox and 50 μL (0.532 mmol) of PhF was added as an NMR standard. The yield of F-Si species was determined by $^{19}F\{^1H\}$ NMR spectrometry (d1=20s). Further heating did not lead to increased F-Si bond formation. GC/MS and ^1H NMR analysis of the reaction mixture show the formation of toluene, only trace toluene was observed when $HSiMe_2Ph$ was used while appx. 1 eq. of toluene per 7 $FSiEt_3$ was detected *via* GC/MS. The difference between the yield of toluene and silylfluoride can be partially explained by the tendency of this substrate to form oligomeric species or reaction with tetrakis(pentafluorophenyl)borate.[4] While F-Si bond formation can be used to estimate TON, typically this number is less (10-20%) than the actual number of C-F bonds broken due to leaching to the borosilicate glass.[5]

Table S1: Catalytic hydrodefluorination of trifluorotoluene with 2

Run	**Silane**	**Eq. Si-F[a]**
1	$HSiPhMe_2$	22
2	$HSiEt_3$	35

[a] Equivalents of F-Si bonds produced per equivalent of **2** assuming no loss of catalyst during filtration

Supplementary Figures

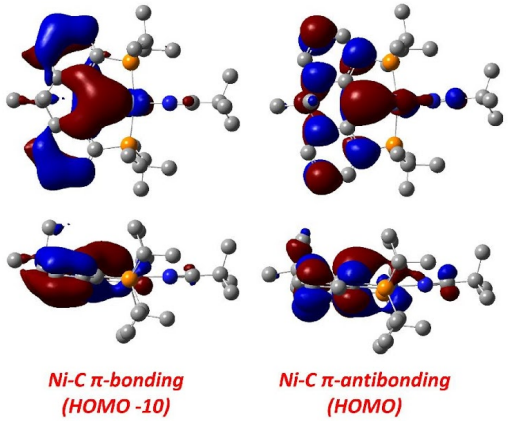

Figure S1. DFT Calculated Molecular Orbitals of II.

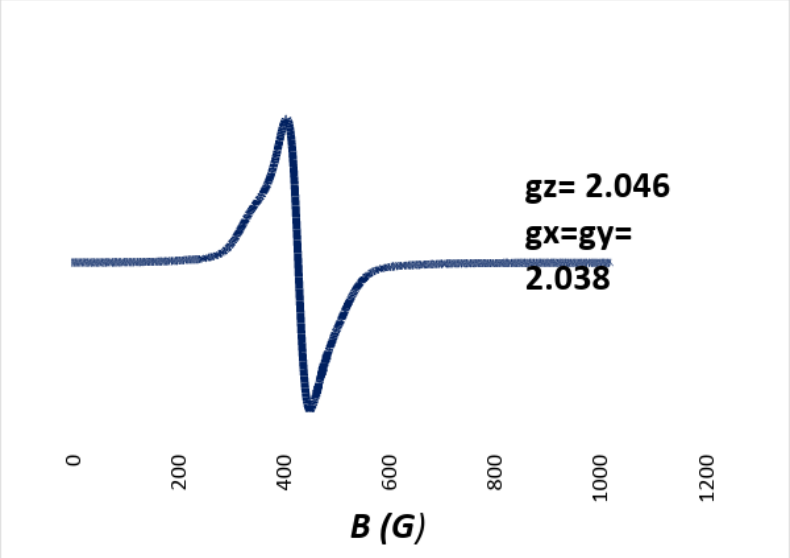

Figure S2. X-Band EPR Spectra of 2_{red} (Toluene glass, 128K)

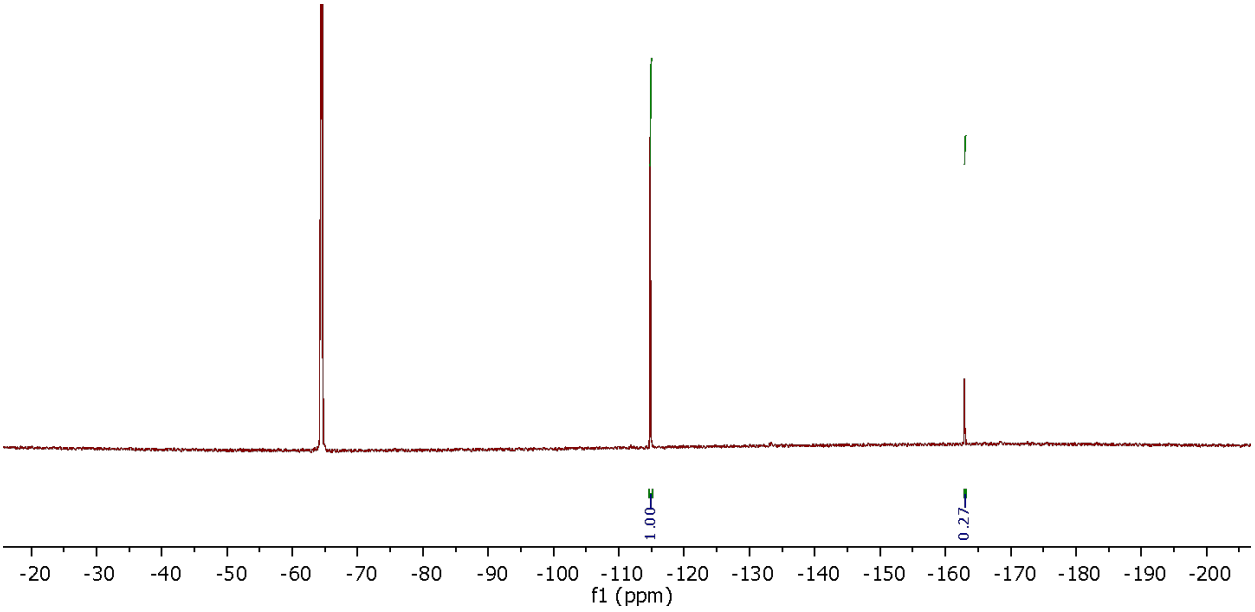
1.00
0.27
-20 -30 -40 -50 -60 -70 -80 -90 -100 -110 -120 -130 -140 -150 -160 -170 -180 -190 -200
f1 (ppm)

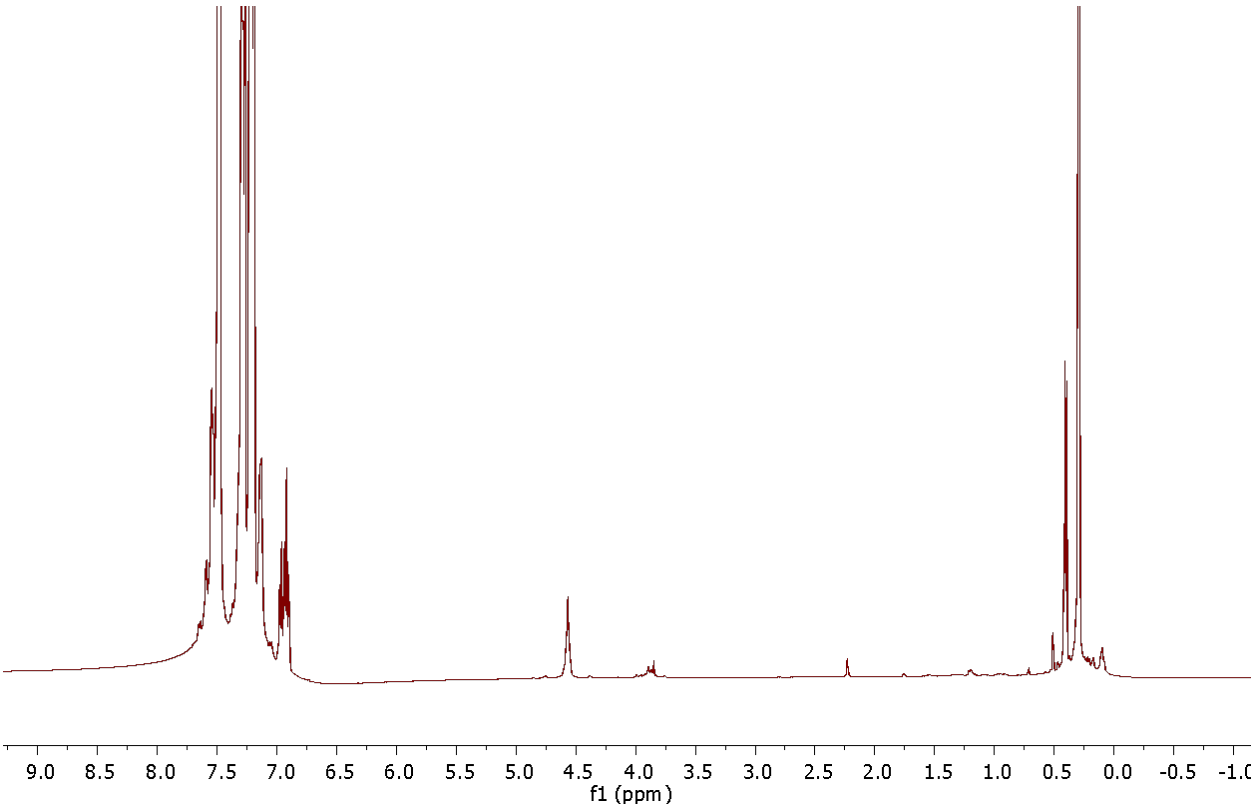
9.0 8.5 8.0 7.5 7.0 6.5 6.0 5.5 5.0 4.5 4.0 3.5 3.0 2.5 2.0 1.5 1.0 0.5 0.0 -0.5 -1.0
f1 (ppm)

Figure S3: $^{19}F\{^{1}H\}$ (top) and ^{1}H NMR Spectra (bottom) of Run 1. FSiMe2Ph (-163 ppm) and toluene (~2.2 ppm) are clearly observable

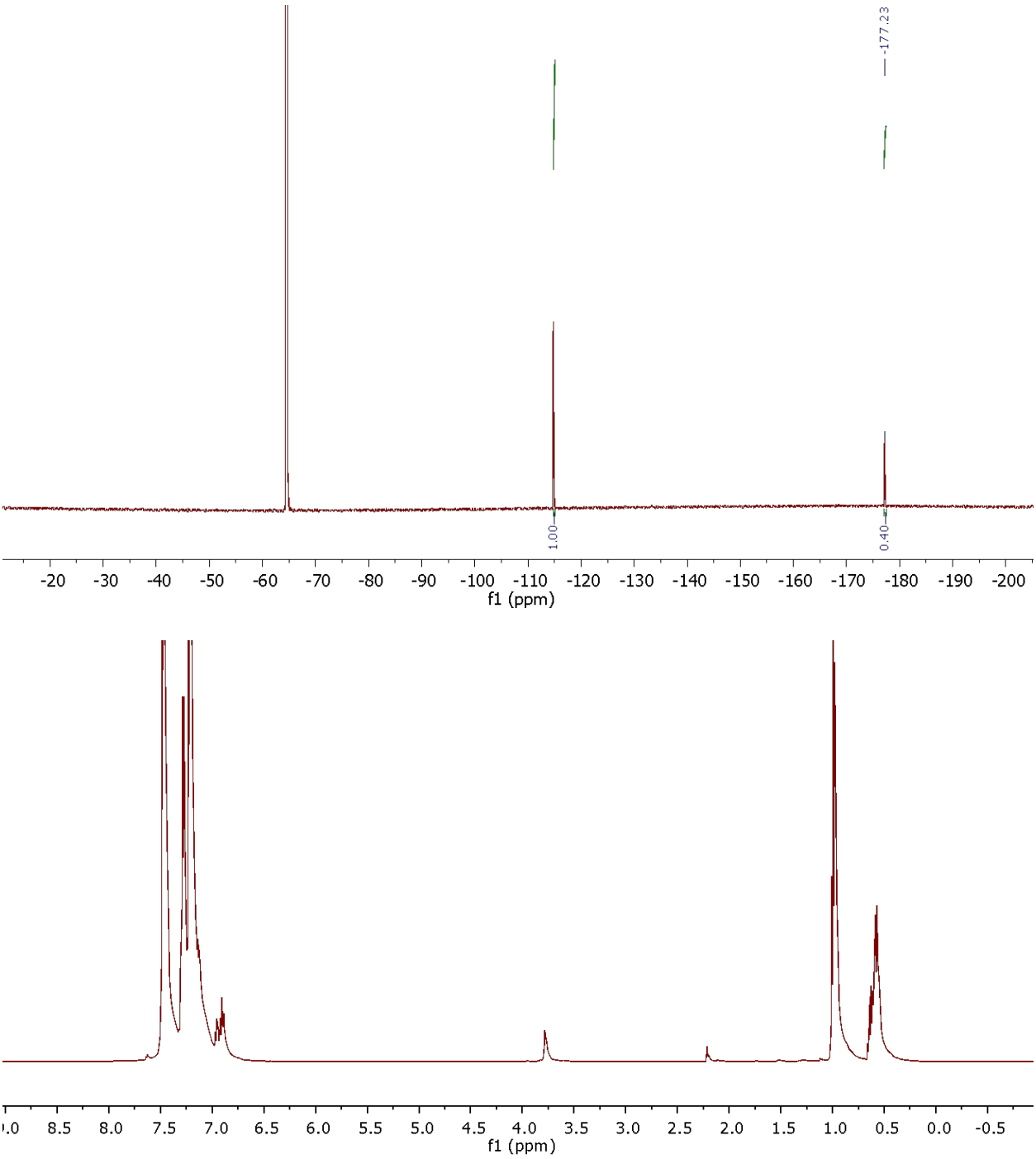

Figure S4: $^{19}F\{^{1}H\}$ (top) and ^{1}H (bottom) NMR Spectra of Run 2. FSiEt3 (-177 ppm) and toluene (~2.2 ppm) are clearly observable

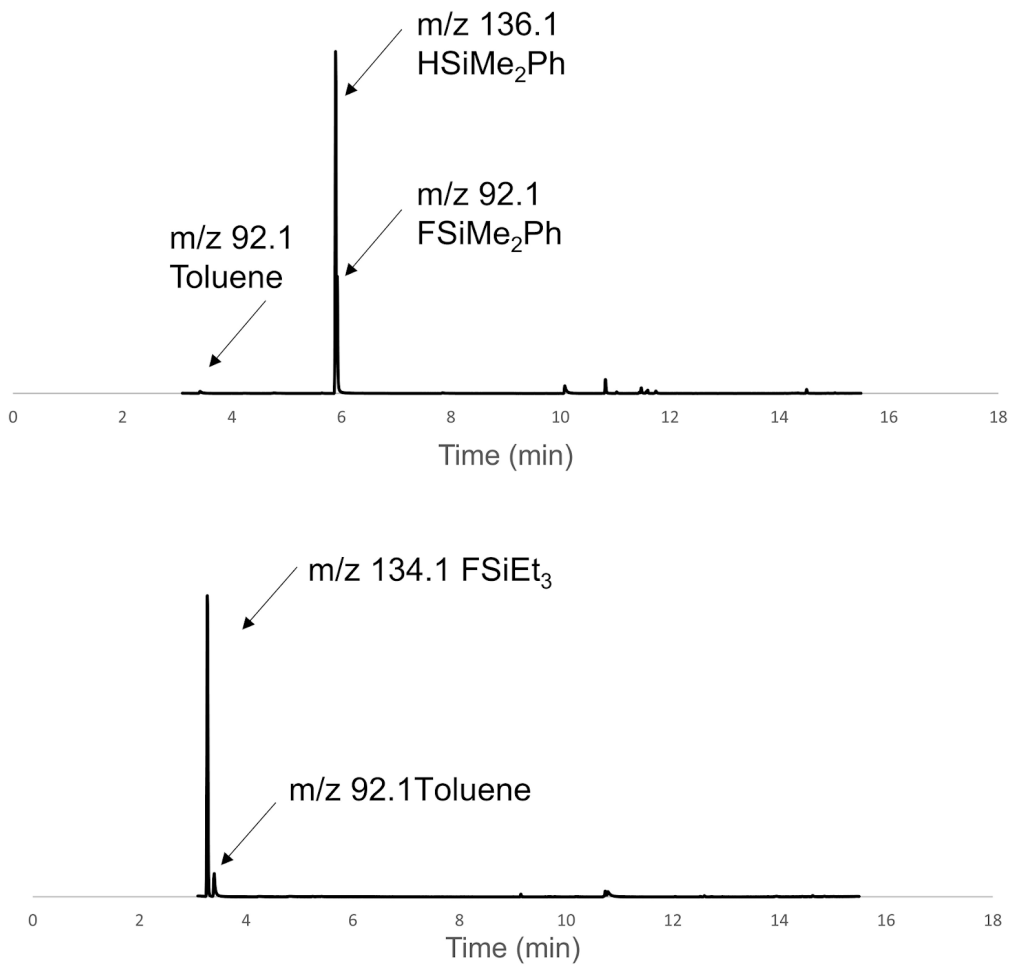

Figure S5: Gas chromatograms of the reaction mixtures of Run 1(top) and Run 2 (bottom)

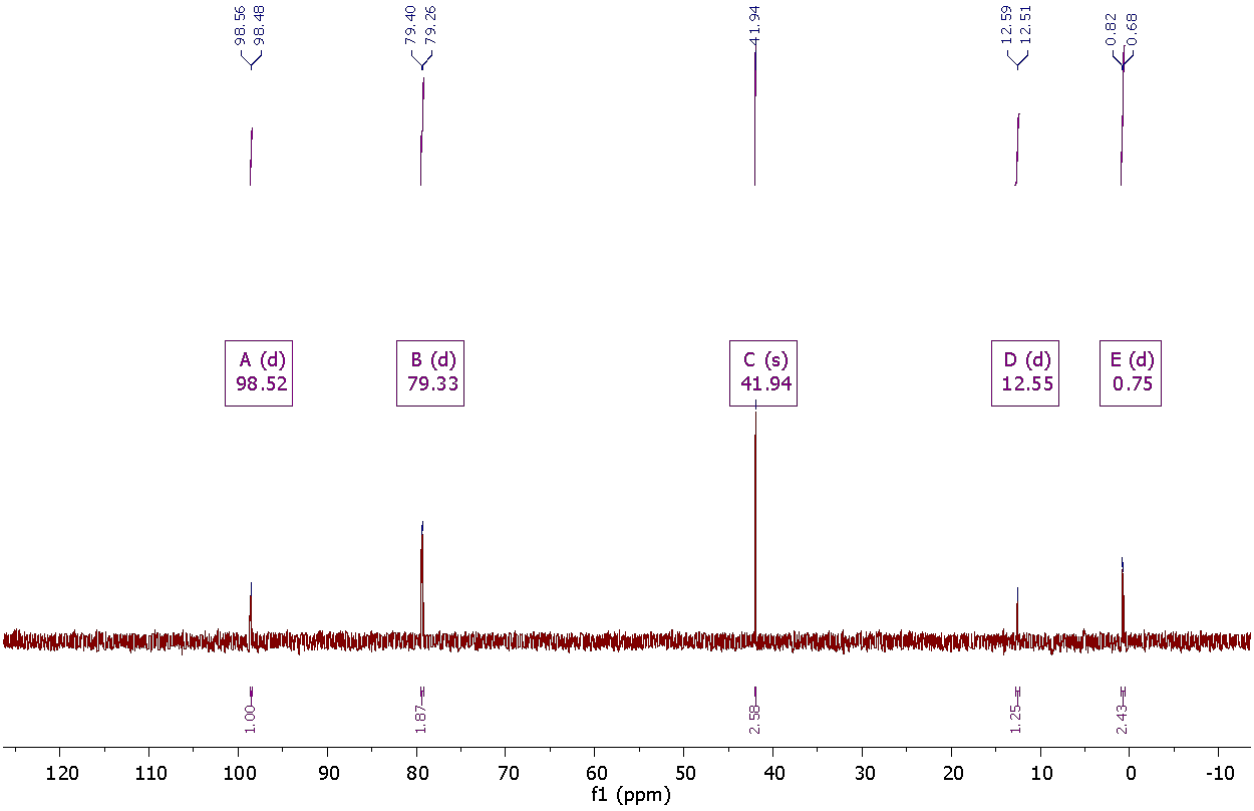

Figure S6. $^{31}P\{^{1}H\}$ NMR Spectrum of the Reaction of 2 with Ammonia in Solution. Reconstituted in C_6D_6. ^{31}P NMR (203 MHz, Benzene-d_6) δ 98.52 (d, J = 16.3 Hz), 79.33 (d, J = 29.0 Hz), 41.94 (4), 12.55 (d, J = 16.3 Hz), 0.75 (d, J = 28.9 Hz).

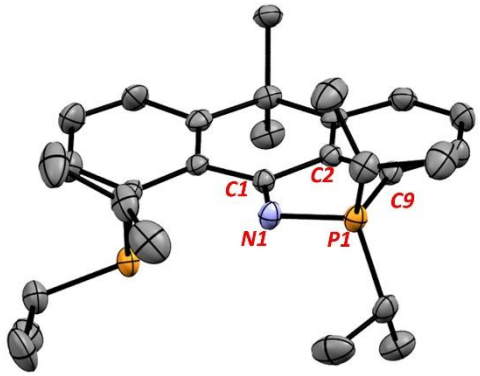

Figure S7. ORTEP diagram for complex 5. Thermal ellipsoids are shown at the 50% probability level. Hydrogen atoms and counter anions are omitted for clarity. Select bond lengths (Å) and angles (degrees) for 4a: N1-C1 1.313(6), N1-P1 1.666(4), C1-C2 1.472(6), C2-C9 1.401(6), C9-P1 1.789(4), C1-N1-P1 109.6(3).

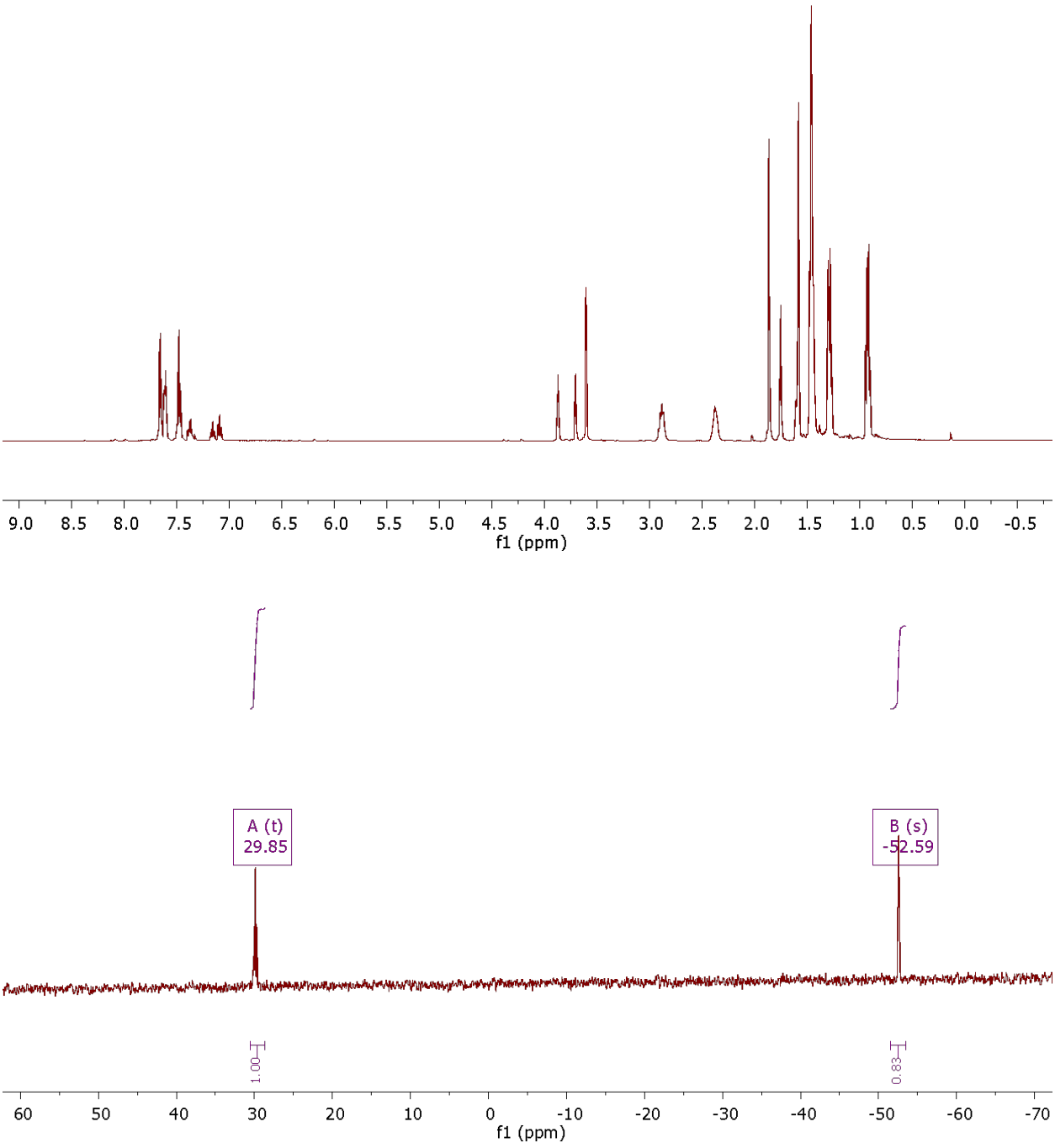

Figure S8. ^{1}H NMR Spectrum (Top) and ^{15}N{^{1}H} NMR Spectrum (Bottom) of ^{15}N-Labelled (98%) 5. Contamination by co-crystallized PhF evident.

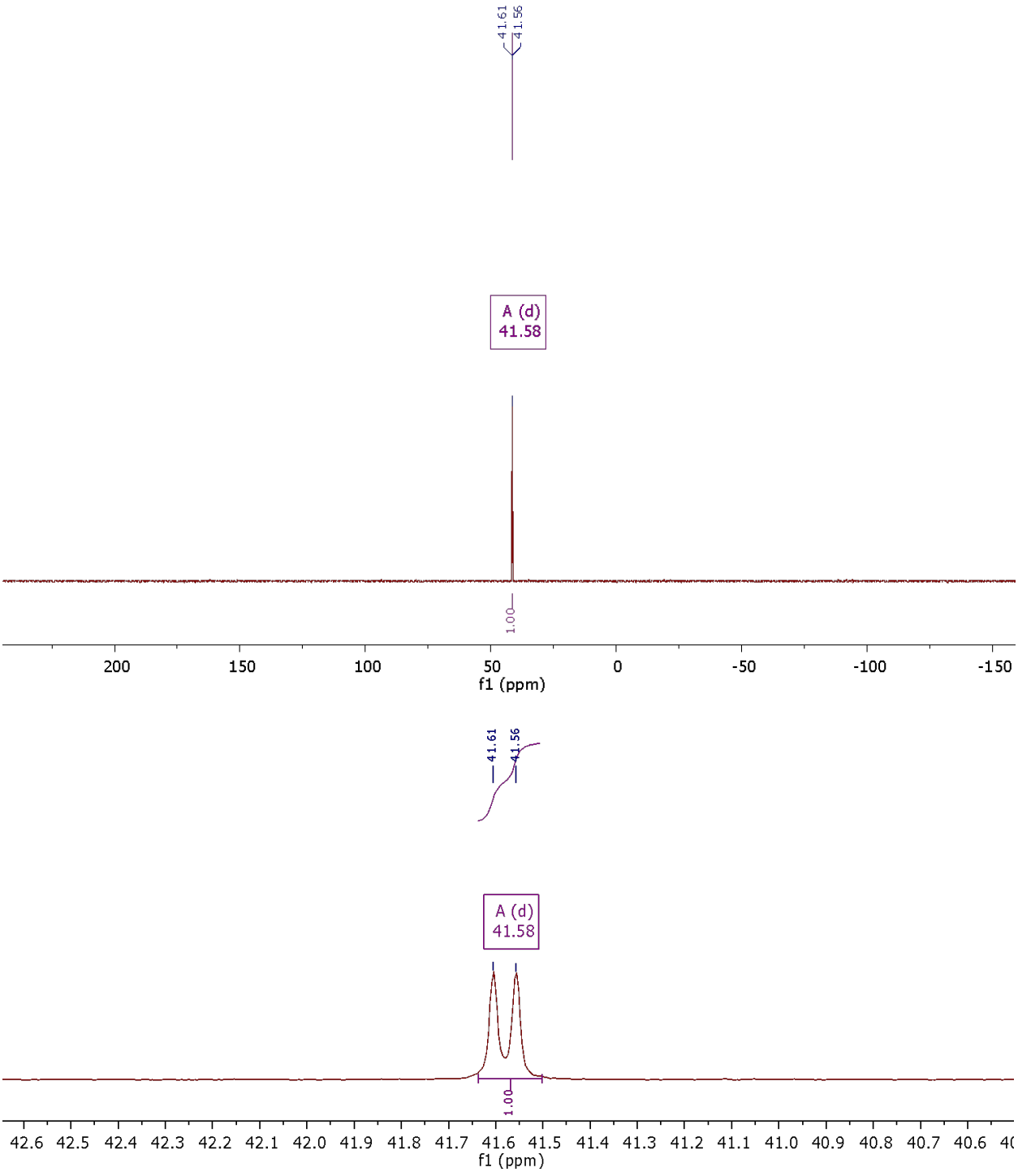

Figure S9. $^{31}P\{^{1}H\}$ NMR Spectrum ^{15}N-Labelled(98%) 5.

Crystal Data Collection and Refinement Parameters

Table S1. Crystal Data Collection and Refinement Parameters for Complexes 2_x

	2	**2_{red}**
formula	$C_{28}H_{40}BrNiP_2,F_6Sb$	$C_{28}H_{40}BrNiP_2$
fw	812.91	577.16
crystal system	monoclinic	triclinic
space group	$P2_{1/n}$	P-1
***a* (Å)**	12.454(11)	11.0190(6)
***b* (Å)**	14.888(13)	11.1636(7)
***c* (Å)**	18.079(18)	13.0424(8)
α (deg)	90	107.237(2)
β (deg)	95.797(14)	98.206(2)
γ (deg)	90	111.768(2)
***V* (Å^3)**	3335(5)	1364.11(14)
Z	4	2
***T* (K)**	173(2)	173(2)
Wavelength (Å)	0.71073	0.71073
ρ_{calcd} (g•cm^{-3})	1.619	1.405
***F*(000)**	1624	602
μ (mm^{-1})	2.719	2.307
crystal size, mm^3	0.14×0.13×0.08	0.27×0.26×0.26
transmission factors	0.6763 − 0.7454	0.6172 − 0.7456
***θ* range (deg)**	1.776 − 24.999	3.040 − 27.564
data/restraints/param	5828/372/362	6218/0/299
GOF	0.976	1.000
R_1 [I > 2σ(I)]	0.0422	0.0334
wR_2 [all data]	0.0921	0.0801
residual density, e/Å^3	1.052 and -0.870	0.509 and -0.513

Table S2. Crystal Data Collection and Refinement Parameters for Complexes 3_x

	3_O	3_{NTs}
formula	$C_{28}H_{40}BrNiOP_2,F_6Sb$[+solvent]	$C_{35}H_{48}BrNNiO_2P_2S,F_6Sb$
fw	828.91	982.10
crystal system	monoclinic	monoclinic
space group	P21/n	P21/c
***a* (Å)**	16.4321(4)	11.7793(5)
***b* (Å)**	14.2612(5)	15.5651(9)
***c* (Å)**	16.6228(5)	20.8787(11)
α (deg)	90	90
β (deg)	110.710(2)	90.523(3)
γ (deg)	90	90
***V* (Å^3)**	3643.7(2)	3827.9(3)
Z	4	4
***T* (K)**	173(2)	173(2)
Wavelength (Å)	0.71073	0.71073
ρ_{calcd} (g•cm^{-3})	1.511	1.704
***F*(000)**	1656	1976
μ (mm^{-1})	2.492	2.442
crystal size, mm^3	0.14×0.13×0.03	0.22×0.21×0.05
transmission factors	0.6117 − 0.7456	0.5972 − 0.7456
***θ* range (deg)**	1.938 − 27.511	2.168 − 25.000
data/restraints/param	8301/381/371	6680/0/462
GOF	0.998	1.010
R_1 [I > 2σ(I)]	0.0450	0.0314
wR_2 [all data]	0.1125	0.0723
residual density, e/Å^3	0.816 and -0.637	0.562 and -0.848

Table S3. Crystal Data Collection and Refinement Parameters for 4 and 5

	4	**5**
formula	$C_{28}H_{45}N_2NiP_2,F_6Sb$	$C_{28}H_{40}NP_2,F_6Sb$[+solvent]
fw	766.06	688.30
crystal system	monoclinic	monoclinic
space group	$P_{21/n}$	P21/n
***a* (Å)**	10.9965(3)	14.4344(11)
***b* (Å)**	16.1517(4)	10.4579(7)
***c* (Å)**	18.8351(4)	22.2043(14)
α (deg)	90	90
β (deg)	101.9790(10)	98.505(3)
γ (deg)	90	90
***V* (Å^3)**	3272.49(14)	3315.0(4)
Z	4	4
***T* (K)**	173(2)	173(2)
Wavelength (Å)	0.71073	0.71073
ρ_{calcd} (g•cm^{-3})	1.555	1.379
***F*(000)**	1560	1400
μ (mm^{-1})	1.553	0.979
crystal size, mm^3	0.28×0.26×0.25	0.18×0.11×0.05
transmission factors	0.6064 − 0.7456	0.5927 − 0.7456
***θ* range (deg)**	3.154 − 25.000	2.690 − 25.000
data/restraints/param	5713/0/372	5790/330/353
GOF	1.016	1.052
R_1 [I > 2σ(I)]	0.0315	0.0432
wR_2 [all data]	0.0812	0.1193
residual density, e/Å^3	1.322 and -0.962	0.560 and -0.697

Table S4. Crystal Data Collection and Refinement Parameters for 6

	6
formula	$C_{31}H_{49}BrNiP_3,F_6Sb$[+solvent]
fw	888.98
crystal system	orthorhombic
space group	Fdd2
***a* (Å)**	38.776(8)
***b* (Å)**	51.519(10)
***c* (Å)**	9.2266(18)
α (deg)	90
β (deg)	90
γ (deg)	90
***V* (Å^3)**	18432(6)
Z	16
***T* (K)**	173(2)
Wavelength (Å)	0.71073
ρ_{calcd} (g•cm^{-3})	1.281
***F*(000)**	7168
μ (mm^{-1})	2.007
crystal size, mm^3	0.18×0.12×0.11
transmission factors	0.6296 − 0.7456
***θ* range (deg)**	2.594 − 25.000
data/restraints/param	7965/400/402
GOF	1.021
R_1 [I > 2σ(I)]	0.0400
wR_2 [all data]	0.0961
residual density, e/Å^3	0.642 and -0.364

Computational Details

All the calculations were conducted using the Gaussian09 program suite.[6] For all calculations the B3PW91[7] functional was used in combination with the SDD basis set and corresponding ECP for Ni,[8] and 6-31G** for all other atoms. The stationary point was confirmed as an energy minimum by the lack of imaginary frequencies.

Table S5. Coordinates for the calculated structure of complex cation 2

Br	9.103000	9.440000	8.268000
C	7.839000	10.002000	4.326000
C	8.756000	9.885000	3.211000
C	8.348000	10.048000	1.862000
C	6.927000	10.409000	1.480000
C	6.013000	10.544000	2.682000
C	6.464000	10.324000	4.009000
C	6.954000	11.762000	0.717000
H	7.345000	12.562000	1.350000
H	5.950000	12.044000	0.389000
H	7.583000	11.691000	-0.174000
C	6.359000	9.299000	0.554000
H	6.969000	9.193000	-0.346000
H	5.342000	9.543000	0.237000
H	6.335000	8.334000	1.068000
C	10.112000	9.567000	3.504000

C	11.032000	9.377000	2.485000
H	12.061000	9.110000	2.701000
C	10.620000	9.531000	1.157000
H	11.334000	9.389000	0.350000
C	9.305000	9.866000	0.858000
H	9.024000	9.981000	-0.184000
C	11.648000	10.742000	5.778000
H	11.768000	10.559000	6.854000
C	11.010000	12.123000	5.597000
H	11.689000	12.894000	5.975000
H	10.068000	12.208000	6.147000
H	10.816000	12.341000	4.541000
C	13.011000	10.653000	5.089000
H	12.937000	10.893000	4.024000
H	13.480000	9.671000	5.193000
H	13.690000	11.386000	5.538000
C	11.276000	7.761000	5.478000
H	12.043000	7.748000	4.692000
C	11.959000	7.577000	6.836000
H	11.235000	7.617000	7.653000
H	12.728000	8.331000	7.027000
H	12.448000	6.598000	6.857000

C	10.269000	6.641000	5.198000
H	10.784000	5.675000	5.204000
H	9.781000	6.751000	4.225000
H	9.497000	6.612000	5.973000
C	5.550000	10.448000	5.093000
C	4.233000	10.816000	4.871000
H	3.537000	10.935000	5.696000
C	3.797000	11.039000	3.561000
H	2.766000	11.323000	3.374000
C	4.674000	10.898000	2.491000
H	4.299000	11.075000	1.488000
C	5.880000	11.592000	7.757000
H	4.807000	11.751000	7.577000
C	6.100000	11.364000	9.255000
H	7.151000	11.166000	9.475000
H	5.508000	10.533000	9.648000
H	5.799000	12.266000	9.798000
C	6.647000	12.819000	7.254000
H	6.311000	13.709000	7.795000
H	6.492000	13.001000	6.186000
H	7.721000	12.703000	7.435000
C	5.495000	8.613000	7.447000

H	6.022000	8.509000	8.405000
C	5.804000	7.377000	6.597000
H	5.397000	6.484000	7.083000
H	6.881000	7.230000	6.475000
H	5.349000	7.449000	5.602000
C	3.994000	8.764000	7.703000
H	3.431000	8.805000	6.765000
H	3.747000	9.649000	8.296000
H	3.633000	7.891000	8.257000
Ni	8.402000	9.751000	6.080000
P	10.435000	9.416000	5.295000
P	6.321000	10.110000	6.714000

Table S6. Coordinates for the calculated structure of II

C	5.47799	7.56459	13.81071
C	5.47566	8.95526	14.16866
C	6.67829	9.71991	14.32745
C	8.00787	8.96809	14.38726
C	7.96283	7.77269	13.43758
C	6.72709	7.05588	13.31618
C	8.14156	8.39898	15.82630
H	8.15208	9.21397	16.55942
H	9.06817	7.82120	15.92350

H	7.29884	7.73982	16.05537
C	9.21153	9.88048	14.12592
H	9.17847	10.31914	13.12326
H	10.14981	9.32830	14.23166
H	9.25305	10.69237	14.85761
C	4.24523	9.63608	14.37912
C	4.17888	10.99538	14.68428
H	3.22127	11.47490	14.87377
C	5.35108	11.74103	14.74534
H	5.32379	12.80578	14.95670
C	6.57916	11.08440	14.57034
H	7.48647	11.67462	14.66304
C	1.65642	9.05030	12.98394
H	0.91348	8.24119	12.94035
C	2.35400	9.13671	11.62326
H	1.62869	9.38189	10.83863
H	2.84292	8.19349	11.36463
H	3.12382	9.91475	11.63210
C	0.93734	10.36182	13.30939
H	1.64099	11.19927	13.31926
H	0.41880	10.33932	14.27267
H	0.18751	10.57456	12.53783

C	2.00329	8.61400	15.90941
H	1.79237	9.68526	16.03193
C	0.68364	7.84295	15.96053
H	0.86107	6.76879	15.84979
H	-0.01897	8.15512	15.18134
H	0.19378	7.99970	16.92885
C	2.94445	8.18104	17.03711
H	2.46785	8.34548	18.01078
H	3.88016	8.74539	17.01387
H	3.19303	7.11764	16.95413
C	6.77142	5.80586	12.64166
C	7.92265	5.32523	12.01831
H	7.90658	4.38148	11.47727
C	9.09080	6.07846	12.06625
H	9.99613	5.73468	11.57507
C	9.08947	7.28174	12.78941
H	10.02048	7.83842	12.84793
C	4.76559	4.58803	10.90322
H	5.59437	3.93544	10.59597
C	3.45405	3.81542	10.75692
H	2.60431	4.43410	11.06401
H	3.43991	2.89597	11.35099

H	3.29845	3.53317	9.70898
C	4.78415	5.82992	10.00919
H	4.65935	5.53894	8.95956
H	5.72442	6.37872	10.10449
H	3.96895	6.51222	10.26933
C	5.24085	3.43936	13.60412
H	4.20417	3.07340	13.61723
C	5.66859	3.72297	15.04816
H	5.65153	2.79864	15.63766
H	5.01226	4.45565	15.52724
H	6.68606	4.12537	15.07681
C	6.13361	2.37351	12.96587
H	7.17569	2.70598	12.93681
H	5.82725	2.11628	11.94711
H	6.09947	1.45270	13.56066
C	1.42664	4.76664	13.88368
C	0.25397	3.88570	14.02370
C	-0.98987	4.63857	13.51124
H	-1.16496	5.55187	14.08609
H	-1.86787	3.99330	13.61560
H	-0.88411	4.90690	12.45642
C	0.08480	3.52345	15.51312

H	0.96572	3.00135	15.89646
H	-0.78218	2.86453	15.62525
H	-0.08146	4.41509	16.12343
C	0.48522	2.60985	13.19150
H	0.61619	2.84323	12.13173
H	-0.38510	1.95418	13.29461
H	1.36717	2.06426	13.53829
N	2.34788	5.47145	13.78768
Ni	3.87473	6.56591	13.68522
P	2.88995	8.46579	14.26773
P	5.14147	5.06206	12.67267

Table S7. Coordinates for the calculated structure of 2_{red}

Br	6.76581	5.03990	3.89493
C	2.78440	3.87434	2.93181
C	2.44461	2.49964	2.64991
C	1.12502	2.07007	2.34069
C	-0.04601	3.04593	2.24523
C	0.37006	4.48602	2.53797
C	1.70750	4.83425	2.87176
C	3.47864	1.52399	2.70445
C	3.21989	0.17419	2.49714
H	4.01591	-0.56140	2.57132

C	1.92065	-0.23831	2.20020
H	1.70113	-1.28884	2.03289
C	0.90076	0.71025	2.12050
H	-0.10345	0.36692	1.88519
C	2.00437	6.19942	3.14067
C	1.03205	7.18873	3.05237
H	1.28191	8.23047	3.23301
C	-0.27632	6.83782	2.71859
H	-1.04915	7.59773	2.64747
C	-0.58694	5.49990	2.47411
H	-1.61305	5.24882	2.21769
C	-1.13102	2.62850	3.26779
H	-1.48165	1.60958	3.07797
H	-1.99830	3.29351	3.21401
H	-0.73563	2.66772	4.28705
C	-0.63052	2.97506	0.81319
H	0.12076	3.27109	0.07514
H	-1.49329	3.63930	0.70544
H	-0.96070	1.95975	0.57350
C	6.25264	1.97140	1.69283
H	7.17591	2.45279	2.04161
C	5.76114	2.72887	0.45577

H	6.48643	2.62554	-0.35928
H	5.63495	3.79452	0.66728
H	4.80138	2.33486	0.10417
C	6.52900	0.50123	1.37328
H	5.63614	0.00962	0.97423
H	6.87404	-0.06625	2.24297
H	7.30934	0.43151	0.60652
C	5.71384	1.26912	4.55278
H	5.55978	0.21999	4.26334
C	7.19917	1.49077	4.84812
H	7.40032	2.54068	5.07686
H	7.84009	1.20209	4.00988
H	7.49247	0.88308	5.71219
C	4.85153	1.56184	5.78468
H	5.14303	0.90252	6.61017
H	3.78668	1.40556	5.58725
H	4.99115	2.59660	6.11337
C	4.32642	7.78702	2.38966
H	3.55172	8.56410	2.45381
C	5.67564	8.39621	2.77837
H	6.45959	7.63440	2.79222
H	5.65207	8.87038	3.76397

H	5.95050	9.16650	2.04829
C	4.35105	7.24748	0.95607
H	4.57802	8.05894	0.25527
H	3.39153	6.80887	0.66586
H	5.12513	6.48116	0.84760
C	3.88430	7.11578	5.27342
H	4.96885	7.22382	5.40726
C	3.38520	6.06785	6.27259
H	3.53140	6.42791	7.29730
H	3.92735	5.12446	6.16171
H	2.31723	5.86578	6.13606
C	3.20220	8.46689	5.49478
H	2.11404	8.37646	5.41860
H	3.53375	9.23260	4.78684
H	3.42885	8.83308	6.50288
Ni	4.55591	4.39276	3.36042
P	5.08189	2.27689	3.11208
P	3.76171	6.43018	3.54326

References

1. E. A. LaPierre, W. E. Piers and C. Gendy, *Organometallics*, 2018, DOI: 10.1021/acs.organomet.8b00440.
2. A. Yoshimura, M. W. Luedtke and V. V. Zhdankin, *The Journal of Organic Chemistry*, 2012, **77**, 2087-2091.
3. E. A. LaPierre, M. L. Clapson, W. E. Piers, L. Maron, D. M. Spasyuk and C. Gendy, *Inorg Chem*, 2018, **57**, 495-506.
4. C. Douvris and O. V. Ozerov, *Science*, 2008, **321**, 1188.
5. V. J. Scott, R. Çelenligil-Çetin and O. V. Ozerov, *Journal of the American Chemical Society*, 2005, **127**, 2852-2853.
6. Gaussian 09, Revision C.01, M. J. Frisch, G. W. Trucks, H. B. Schlegel, G. E. Scuseria, M. A. Robb, J. R. Cheeseman, G. Scalmani, V. Barone, G. A. Petersson, H. Nakatsuji, X. Li, M. Caricato, A. Marenich, J. Bloino, B. G. Janesko, R. Gomperts, B. Mennucci, H. P. Hratchian, J. V. Ortiz, A. F. Izmaylov, J. L. Sonnenberg, D. Williams-Young, F. Ding, F. Lipparini, F. Egidi, J. Goings, B. Peng, A. Petrone, T. Henderson, D. Ranasinghe, V. G. Zakrzewski, J. Gao, N. Rega, G. Zheng, W. Liang, M. Hada, M. Ehara, K. Toyota, R. Fukuda, J. Hasegawa, M. Ishida, T. Nakajima, Y. Honda, O. Kitao, H. Nakai, T. Vreven, K. Throssell, J. A. Montgomery, Jr., J. E. Peralta, F. Ogliaro, M. Bearpark, J. J. Heyd, E. Brothers, K. N. Kudin, V. N. Staroverov, T. Keith, R. Kobayashi, J. Normand, K. Raghavachari, A. Rendell, J. C. Burant, S. S. Iyengar, J. Tomasi, M. Cossi, J. M. Millam, M. Klene, C. Adamo, R. Cammi, J. W. Ochterski, R. L. Martin, K. Morokuma, O. Farkas, J. B. Foresman, and D. J. Fox, Gaussian, Inc., Wallingford CT, 2016.
7. J. P. Perdew and Y. Wang, *Physical Review B*, 1992, **45**, 13244-13249.
8. M. Dolg, U. Wedig, H. Stoll and H. Preuss, *The Journal of Chemical Physics*, 1987, **86**, 866-872.